Scour Development and Possible Effects of Momentary Liquefaction in Inundated Coastal Areas During Hurricane Michael

Matthew Florence[1]; Nina Stark, Ph.D., M.ASCE[2]; and Andrew Kennedy, Ph.D., M.ASCE[3]

Abstract: Scour holes around slender piles were measured in areas inundated during Hurricane Michael and were compared with scour hole depths estimated from existing scour prediction equations. Despite testing a wide range of feasible input parameters, some measured scour depths could not be predicted by five common scour prediction equations (one wave only, three current only, one wave and current equation). Current only equations yielded the best prediction rate despite the site being in a wave-dominated environment. The scour depths that were not accurately predicted by the equations tended to be underpredictions despite the range of input values. A range of factors were considered that might have caused these differences. Momentary liquefaction was investigated as one possible explanation to some of the discrepancies between observed and predicted scour depths using laboratory tests and field measurements. The results suggested that momentary liquefaction of the top layer of sediment is possible for wave heights of approximately 0.83 m in 1.3 m of water depth, indicating that momentary liquefaction of sediments was possible during Hurricane Michael with 2 m waves in 3.5 m of water and therefore presents one possible explanation for the observed mismatch between the scour predictions and observations. **DOI: 10.1061/(ASCE)WW.1943-5460.0000699**.

Introduction

Hurricane Michael made landfall on October 9, 2018, near Mexico Beach, FL. The resulting destruction to infrastructure resulted in $25 billion in damages (NOAA 2019). The piles supporting onshore structures were inundated and subjected to waves and currents driven by the storm for approximately 3 h (Kennedy et al. 2020). As a result, scour holes were observed in areas that were normally not at risk of scour (onshore piles located approximately 100 m or more from the shoreline). The prediction of scour at onshore locations during extreme inundation events (e.g., hurricane or tsunami) is not as common or as researched compared with scour in riverine or offshore environments (Borga et al. 2017; McGovern et al. 2019). McGovern et al. (2019) tackled this gap in knowledge by designing experiments with a specialized pneumatic long-wave generator and a detailed laboratory setup in order to observe scour development in real time, albeit scaled down to a 1:50 Froude scale. Borga et al. (2017) determined that only two equations adequately described scour around a building foundation (and not a slender pile) resulting from storm surge using the flow, building, and soil characteristics as input parameters.

It could be speculated that the lack of easily accessible equations predicting scour during inundation events is because these processes are the same or similar to offshore or riverine scour processes. However, Borga et al. (2017) stated that limited inundation time, poorly defined flow geometry, and variability in flow velocity may create significant differences between riverine and offshore scour processes compared with onshore inundation scour processes. Floating debris and rapid changes in water depth are other factors that may be unique to storm-based inundation events (Kennedy et al. 2020; USGS 2020). Additionally, onshore soils (onshore being defined for this study as located between 100 and 350 m from the shoreline during nonstorm conditions) have not been exposed to energetic hydrodynamic conditions (i.e., may not have developed natural armoring) and may have increased gas content compared with riverine or offshore sediments, both of which may increase the risk of scour for these sediments (Mory et al. 2007; Vanoni 2014).

There are several scour prediction equations for riverine and subaqueous environments (e.g., Froehlich 1988; FHWA 2012; others presented in Sumer and Fredsøe 2002). However, it is uncertain how accurately these equations predict scour depth for inundated onshore locations, especially since wave-induced scour is of interest during storm events. It is known that scour around slender piles caused by unbroken waves is dictated by the Keulegan–Carpenter (KC) number and controlled by lee-wake and horseshoe vortices (Sumer et al. 1992, 1993; Kobayashi and Oda 1994; Sumer and Fredsøe 2002). However, the KC number, lee-wake vortices, and horseshoe vortices may not be the only wave-related processes involved in scour mechanics. Wave-induced excess sediment pore-pressure gradients are known to occur in the uppermost (~50 cm) layer of sediment in the nearshore zone (e.g., Sakai et al. 1992; Raubenheimer et al. 1998; Sumer and Fredsøe 2002; Mory et al. 2007; Guest and Hay 2017). These excess pore-pressure gradients have been observed to cause liquefaction of the soil, which may facilitate scour under a significantly smaller bed shear stress. Despite this knowledge, several common sediment transport and scour prediction equations do not consider the role of wave-induced sediment pore-pressure gradients in scour processes (Froehlich 1988; Sumer and Fredsøe 2002; FHWA 2012).

[1]Ph.D. Student, Dept. of Civil and Environmental Engineering, Virginia Tech., 200 Patton Hall, Blacksburg, VA 24061 (corresponding author). ORCID: https://orcid.org/0000-0003-3876-173X. Email: matthf6@vt.edu

[2]Associate Professor, Dept. of Civil and Environmental Engineering, Virginia Tech., 200 Patton Hall, Blacksburg, VA 24061. ORCID: https://orcid.org/0000-0001-9484-069X. Email: ninas@vt.edu

[3]Professor, Dept. of Civil and Environmental Engineering, Univ. of Notre Dame, 156 Fitzpatrick Hall, Notre Dame, IN 46556. Email: andrew.kennedy@nd.edu

Note. This manuscript was submitted on August 27, 2020; approved on November 7, 2021; published online on December 22, 2021. Discussion period open until May 22, 2022; separate discussions must be submitted for individual papers. This paper is part of the ***Journal of Waterway, Port, Coastal, and Ocean Engineering***, © ASCE, ISSN 0733-950X.

Yamamoto et al. (1978) showed that excess sediment pore pressures in a porous media experience attenuation as a function of wave period and soil depth (among other geotechnical parameters). This excess pressure attenuation coupled with a sediment-depth-dependent phase lag of a pressure signal (Raubenheimer et al. 1998; Mory et al. 2007; Stark and Quinn 2015; Guest and Hay 2017) can cause an upward-directed vertical excess pore-pressure gradient that is sufficiently large to overcome the effective stress of the soil. When the effective stress of the soil is zero, the soil has no contact force between the particles (Terzaghi et al. 1996; Holtz et al. 2017). In the absence of contact forces, the soil no longer behaves like a granular solid and instead behaves like a fluid or suspension. Thus, the sediment can be mobilized and transported more easily; this process has been referred to as momentary liquefaction (Sakai et al. 1992; Mory et al. 2007). Momentary liquefaction may have importance with respect to scour processes, as a liquefied soil will move under significantly smaller shear stresses (Shields 1936; Sakai et al. 1992; Yeh and Mason 2014).

The concept of momentary liquefaction is illustrated in Fig. 1. In still water [Fig. 1(a)], the pressure in the sand is hydrostatic, and the sand can support the rock with some deformation. Under the crest of a wave [Fig. 1(b)], an excess vertical pore-pressure gradient directed downward (i.e., decreasing excess pore pressure with increasing sediment depth) develops and acts to strengthen the sand. In theory, under the crest of a wave, the sand is as strong as or stronger than still water conditions. Underneath the trough of the wave [Fig. 1(c)], a vertical excess pore-pressure gradient, with excess pore pressure increasing with increasing sediment depth, causes the soil to weaken. In this weakened state, the soil may be unable to support the rock, and it begins to sink into the sand bed. For a more detailed explanation of momentary liquefaction, please see Sakai et al. (1992).

The purpose of this study is to determine the feasibility of using traditional scour equations with input parameters accessible, or at least fairly predictable, for rapidly inundated onshore (100–350 m from the shoreline) sediments where scour is likely to have occurred, and to discuss the possible sources of disagreement, if any, between field-measured and equation-predicted scour depths. Furthermore, momentary liquefaction is explored in detail as one possible explanation of increased scour depths. The sediments in question represent drier and looser sediments compared with the sediments used for the development of most scour equations (Froehlich 1988; Sumer and Fredsøe 2002; FHWA 2012). These drier sediments are at a larger risk of momentary liquefaction compared with saturated sediments owing to the phenomenon's sensitivity to gas content (Sumer and Fredsøe 2002; Mory et al. 2007).

For this purpose, (1) scour holes created around slender piles from Hurricane Michael were measured and sediment samples were taken in Mexico Beach, FL; (2) from a range of hydrodynamic and geotechnical parameters, scour equations were used to predict a range of possible scour depths to compare to each measured scour hole; (3) simple laboratory experiments were designed to test the excess pore-pressure gradients required to induce liquefaction in the sediment samples taken from Mexico Beach, FL; and (4) field measurements of excess pore-pressure gradients were taken at a site (Cannon Beach, Yakutat, AK) with comparable sand conditions to determine the range of feasible pore-pressure gradients that exist in the field. As no excess pore-pressure measurements were conducted at the locations of interest during the storm, the laboratory experiments (3) and the field measurements of excess pore-pressure gradients (4) were used in conjunction to test the feasibility of momentary liquefaction and thus support or reject whether momentary liquefaction could have enhanced scour at Mexico Beach, FL, during Hurricane Michael.

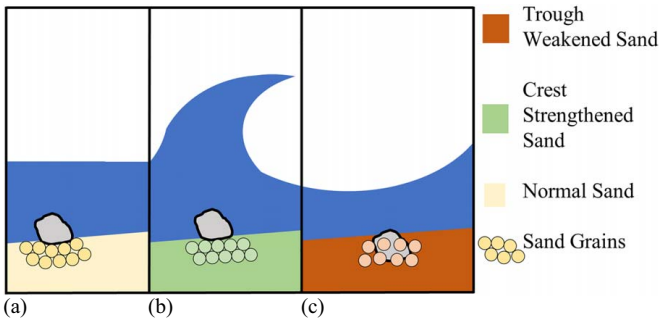

Fig. 1. (Color) Conceptual sketch of impact of liquefaction from vertical pressure gradients induced by the different wave phases on a rock supported by the seabed: (a) No wave—underneath still water, the rock rests on top of the sand bed with the sand bed providing sufficient sediment strength to support the rock; (b) Wave crest—underneath the crest of a wave, pressure gradients within the sand bed can develop in such a way that the soil may be strengthened more than the no wave scenario due to the resulting excess pressure gradients pushing the sand grains together. In this case, the rock remains well supported; and (c) Wave trough—underneath the trough of a wave, excess pressure gradients within the sand bed can develop in such a way that the soil is weakened and, in some cases, liquefied. This causes the rock to sink into the sand bed as the weakened soil cannot support the rock's weight.

Regional Context

Mexico Beach [see white circles in Figs. 2(a and b)] is located on the coast of the panhandle of Florida, United States, approximately 120 km southwest of the state capital of Tallahassee. The state of Florida is part of a larger land mass called the Florida Platform, forming a plateau that is predominantly submerged and spans from the Gulf of Mexico to the Atlantic Ocean. The western edge of the platform is delineated by a steep change in water depth from approximately 90 to 3,000 m (Bostick et al. 2005). The geology of the Florida Platform is comprised of Pliocene, Pleistocene, and Holocene epoch rocks. As a result, siliciclastic sediment deposits cover most of the state (FDEP 2019). Mexico Beach, FL, contains mainly Holocene rock, and the beaches are comprised of a silica-based sand with the nearest coral reef structure approximately 1.8 km from the shoreline (MBARA 2020). The Jackson Bluff-, Intracoastal-, and Bruce Creek Limestone rock formations underlay Mexico Beach, FL at approximate depths of 32, 80, and 135 m, respectively, below the ground surface, and are unlikely to have affected the sediment pore pressures discussed in this study (Schmidt and Clark 1980).

In situ measurements of water depths and wave heights were collected by a United States Geological Survey (USGS) wave gage (FLBAY03283) located on the pier in Mexico Beach, FL, during Hurricane Michael (Kennedy et al. 2020). The point gage was located approximately 55 m inland from the normal shoreline and at an elevation of 2.12 m North American Vertical Datum of 1988 (NAVD88). The gage only reported values when the water level rose sufficiently to inundate the gage. According to Kennedy et al. (2020), the gage reported a maximum significant wave height of 2 m and a maximum instantaneous water depth of 5.2 m NAVD88. Additionally, high-water marks throughout Mexico Beach, FL, reported water elevations of around 5.8 m NAVD88, approximately 300 m inland in Fig. 2(d) (USGS 2020). These measurements will serve as guides for the input parameters used for the scour prediction equations discussed in the Methods section. Elevations in

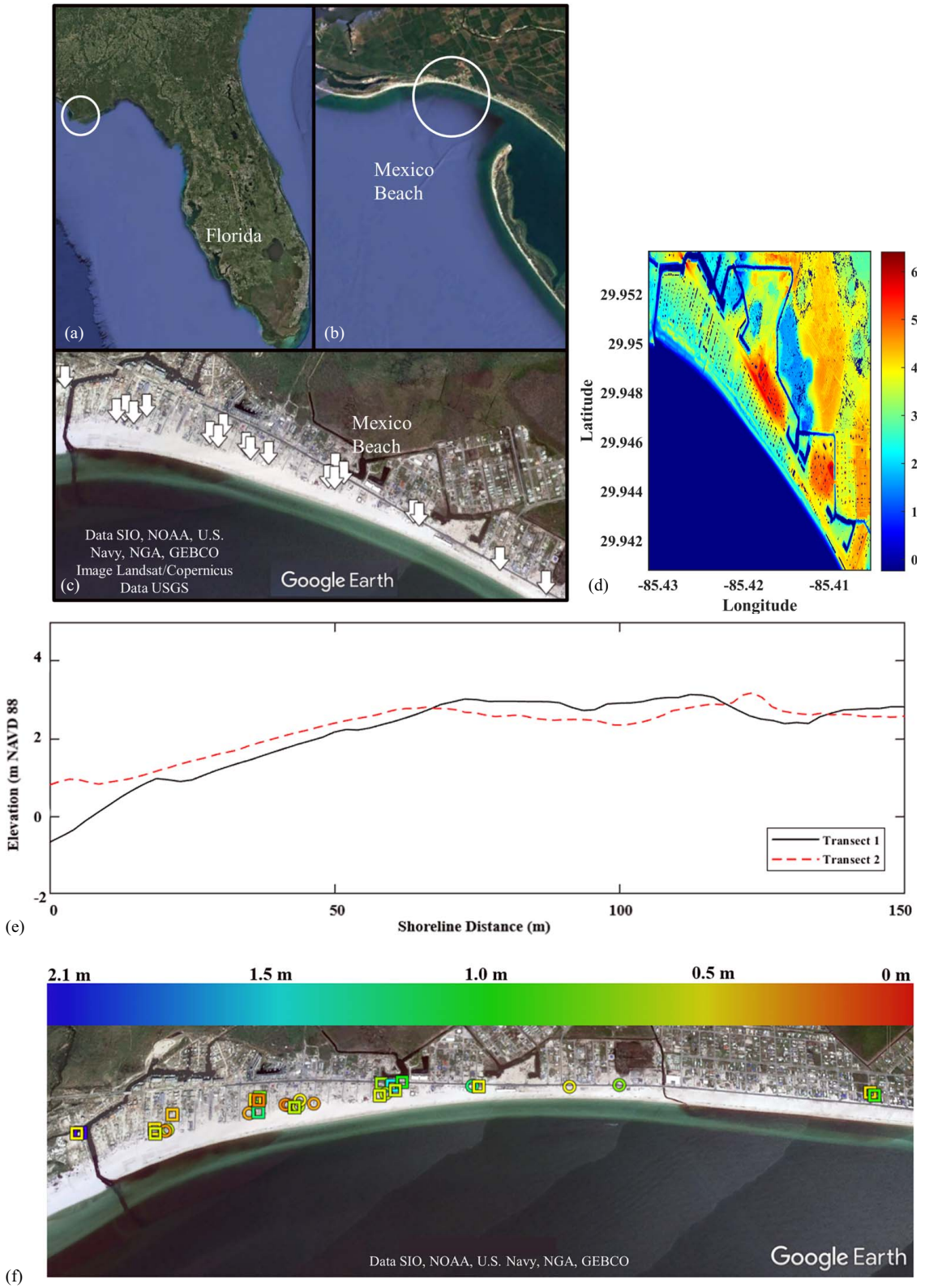

Fig. 2. (Color) (a) Location of Mexico Beach (white circle) in Florida, United States; (b) Close-up image showing Mexico Beach, FL; (c) A zoomed in image of Mexico Beach, FL. The white arrows depict the locations where scour hole measurements were taken (map © 2021 Google; Data SIO, NOAA, US Navy, NGA, GEBCO; Image Landsat/Copernicus Data USGS); (d) Local elevation of areas in Mexico Beach, FL, in 2017. Regions shown are where scour hole measurements were made. Elevations are in meters from NAVD88. Here a negative sign indicates west longitude; (e) Two representative cross-shore transects taken from the nominal shoreline to 150 m inland. Both transects were measured in the western end of Mexico Beach, FL, after Hurricane Michael; and (f) Locations of scour holes measured in Mexico Beach, FL. The shape of the point represents the pile shape around which the scour hole formed (i.e., square point for a square pile). The color of each point shows the depth of scour measured with 2.1 m in blue being the maximum value. The color bar displays a minimum of 0 m, but the measured minimum scour depth was 0.24 m (map © 2021 Google; Data SIO, NOAA, US Navy, NGA, GEBCO).

the Mexico Beach, FL, area 1 year prior to Hurricane Michael are shown in Fig. 2(d). The reader is directed to Kennedy et al. (2020) for an additional elevation map around the time of the event, as well as two cross-shore transects of two streets in Mexico Beach, FL. Additionally, two representative cross-shore transects of the west end of the Mexico Beach, FL, area from shoreline to 150 m inland after Hurricane Michael are shown in Fig. 2(e). Measured scour depths around piles after Hurricane Michael are shown in Fig. 2(f).

Significant changes to geomorphology (Fig. 3) as well as scour around structures (Fig. 4) were observed in response to inundation and hydrodynamic forcing (Kennedy et al. 2020). Figs. 3(a and b) show the complete destruction of the pier and surrounding houses in Mexico Beach, FL, and Figs. 3(c and d) show a significant breach event along the nearby Cape San Blas, FL.

Methods

Scour Holes and Prediction Equations

A total of 30 scour holes of varying sizes were measured [locations shown in Fig. 2(c) by white arrows; see also a close-up of two piles shown in Fig. 4] during a rapid field reconnaissance at Mexico Beach, FL (Kennedy et al. 2020). All scour hole measurements were collected in the Mexico Beach, FL, area [Fig. 2(c)]. Table 1 lists the pile dimensions, shape, and associated scour depth as measured in the field. Fig. 2(d) shows the local elevation in meters with respect to NAVD88 1 year prior to Hurricane Michael (NOAA 2020). Ground elevations around piles measured prestorm ranged from 1 to 6 m NAVD88. Fig. 2(f) shows the relative scour depth in meters (the color of each point shows the depth of scour measured, blue representing maximum scour depth) as well as the shape of the pile (e.g., square data point for square pile).

Five scour prediction equations (Table 2) were chosen from the literature to compare the predictions with the actual measurements. The Froehlich (1988), Froehlich (1988) Design, and HEC-18 (FHWA 2012) equations were developed for cohesionless, riverine (current only) scour conditions. The Sumer et al. (1992) equation was developed for wave-induced scour as indicated by the reliance on the *KC* number. The Sumer and Fredsøe (2001) equation accounts for wave orbital velocity and current velocity (i.e., wave and current conditions). These equations require as input parameters, (1) median grain size and (2) hydrodynamic conditions (e.g., flow velocity, Froude number, and water depth) including the wave characteristics (e.g., wavelength, wave period, wave height, and *KC* number). It should be noted that the fifth equation (Sumer and Fredsøe 2001) requires the scour depth from a current only prediction equation as an input.

The water depths that the Froehlich (1988), FHWA (2012), Sumer et al. (1992), and Sumer and Fredsøe (2001) equations were calibrated for were 0.6–19.5, 0.1–0.55, 0.4, and 0.4 m, respectively. The median grain sizes used for the development of the equations were 0.008–90, 0.45–5.35, 0.18–0.58, and 0.2 mm, respectively. Wave height ranges were not explicitly stated in either of the wave-based studies (Sumer et al. 1992; Sumer and Fredsøe 2001). Wave periods for the two wave-based equations ranged from 1.2–4.5 and 2.5–3.3 s, respectively. The *KC* number for the Sumer et al. (1992) and Sumer and Fredsøe (2001) equations ranged from 4.4–102 and 4–26, respectively. The large wave periods and *KC* numbers (e.g., $KC = 5{,}626$) found in the test conditions from Sumer et al. (1992) were not used here as they pertain to tidal scale effects. Pile diameters for all equations tested ranged from 0.29–19.5, 0.05–0.35, 0.01–0.2, and 0.3–0.9 m, respectively. Flow velocities for all equations except for Sumer et al. (1992) were 0.15–3.6, 0.28–0.8, and 0–0.84 m/s, respectively. Orbital velocities for the two wave-based equations were 0.11–0.53 and 0.16–0.24 m/s, respectively. Measured pile shapes were either square or round while Sumer et al. (1992) and Sumer and Fredsøe (2001) only tested round piles. The conditions in which these equations were tested as well as the respective input parameters used for this study are presented in Table 3. Additional input parameters required for these equations (but not provided readily in the respective studies) are listed in Tables 4 and 5.

The inherent assumptions of these equations are sufficient time of inundation and scouring to achieve the maximum scour depth, relatively simple flow geometry (i.e., flow around a single slender pile), and the flow conditions being constant in time. These conditions may contrast those of storm-induced inundation events (Borga et al. 2017). Only scour around slender piles was considered in this study to avoid adding further uncertainties. This is in line with the scour prediction equations used. Thus, sites with more complex structure interactions, such as Fig. 4(b), were omitted from analysis. Due to limitations in both the study's scope and the availability of in situ measurements, the list of scour equations used was limited. This resulted in the omission of scour prediction equations that may have behaved better than the ones tested here

Fig. 3. (Color) Before and after Hurricane Michael satellite images of Mexico Beach and Port St. Joe, FL: (a and b) the destruction of multiple houses and the pier in Mexico Beach, FL; (c and d) a breach event at Cape San Blas in Port St. Joe. (Maps © 2021 Google.)

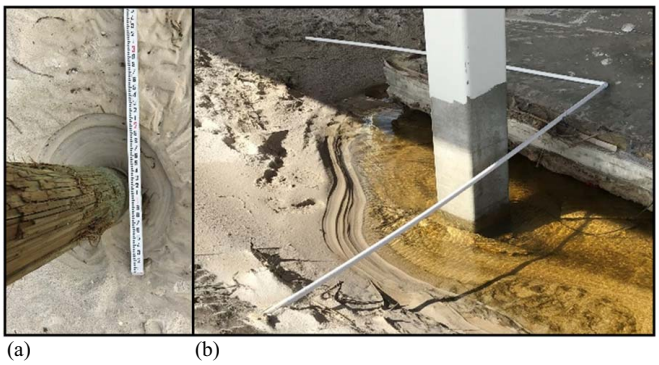

Fig. 4. (Color) Measurements of scour holes developed around piles in Mexico Beach, FL. Increments are in decimal feet: (a) the conditions for which most scour equations were developed; and (b) the pile will have more complex flow geometry than what most scour equations represent due to the nearby construction. Piles similar to (b) have not been considered in this study as they are subjected to different conditions than the predictive equations used here. (Images by Matthew Florence.)

Table 1. Approximate locations of scour holes and the respective pile width, shape, scour depth, scour depth divided by pile width, and elevation (NAVD88) measured at different locations in Mexico Beach, FL

Latitude (north)	Longitude (west)	Pile width (m)	Pile shape	Measured scour depth (m)	Measured scour depth/pile width	Ground elevation (m; from NAVD88)
29°57′10.11″	85°25′48.78″	0.3	Square	2.1	7.0	2.9
29°56′43.81″	85°24′54.00″	0.3	Square	1.5	5.0	2.7
29°56′34.96″	85°24′41.24″	0.2	Circle	1.2	6.0	2.5
29°56′54.28″	85°25′18.53″	0.3	Square	1.2	4.0	2.4
29°56′43.81″	85°24′54.00″	0.3	Square	1	3.3	2.7
29°55′49.77″	85°23′38.31″	0.3	Square	0.92	3.1	N/A[a]
29°56′56.06″	85°25′17.13″	0.3	Square	0.76	2.5	3.0
29°56′19.02″	85°24′17.50″	0.3	Circle	0.75	2.5	3.8
29°56′45.29″	85°24′55.48″	0.28	Square	0.7	2.5	3.1
29°56′43.26″	85°24′56.02″	0.3	Circle	0.64	2.1	2.4
29°56′51.10″	85°25′12.25″	0.3	Square	0.64	2.1	2.6
29°56′50.81″	85°25′11.52″	0.3	Circle	0.63	2.1	2.6
29°57′1.29″	85°25′35.31″	0.29	Circle	0.6	2.1	2.4
29°56′42.77″	85°24′54.10″	0.3	Square	0.6	2.0	3.0
29°57′2.00″	85°25′37.12″	0.3	Square	0.58	1.9	3.0
29°56′43.64″	85°24′57.24″	0.3	Square	0.56	1.9	2.7
29°56′24.22″	85°24′25.73″	0.25	Circle	0.52	2.1	2.4
29°56′34.19″	85°24′40.23″	0.2	Square	0.52	2.6	2.5
29°56′50.81″	85°25′11.52″	0.3	Circle	0.5	1.7	2.6
29°57′10.11″	85°25′48.78″	0.3	Square	0.5	1.7	2.9
29°57′2.75″	85°25′36.73″	0.3	Square	0.45	1.5	2.7
29°55′49.77″	85°23′38.31″	0.3	Square	0.44	1.5	N/A[a]
29°56′56.06″	85°25′17.13″	0.3	Square	0.44	1.5	3.0
29°57′3.16″	85°25′32.43″	0.2	Square	0.38	1.9	2.7
29°56′55.05″	85°25′20.14″	0.46	Circle	0.34	0.7	2.8
29°56′49.56″	85°25′8.75″	0.3	Circle	0.33	1.1	2.4
29°57′1.29″	85°25′35.31″	0.29	Circle	0.3	1.0	2.4
29°56′52.10″	85°25′13.03″	0.27	Circle	0.28	1.0	2.9
29°56′52.10″	85°25′13.03″	0.27	Circle	0.26	1.0	2.9
29°56′56.06″	85°25′17.13″	0.3	Square	0.24	0.8	3.0

Note: Duplicate latitudes and longitudes represent a location with multiple piles that displayed scour.
[a]N/A indicates that the pile location was outside the bounds of the elevation map [Fig. 2(d)].

Table 2. Scour prediction equations from the respective studies

Equation name	Equation
Froehlich (1988)	$y_s = 0.32b\phi \mathrm{Fr}_1^2 \left(\frac{b_e}{b}\right)^{0.62} \left(\frac{y_o}{b}\right)^{0.46} \left(\frac{b}{D_{50}}\right)^{0.08}$
Froehlich (1988) Design	$y_s = 0.32b\phi \mathrm{Fr}_1^2 \left(\frac{b_e}{b}\right)^{0.62} \left(\frac{y_o}{b}\right)^{0.46} \left(\frac{b}{D_{50}}\right)^{0.08} + b$
HEC-18 (FHWA 2012)	$y_s = 2.0 y_o K_1 K_2 K_3 K_4 \left(\frac{b}{y_o}\right)^{0.65} \mathrm{Fr}_1^{0.43}$
Sumer et al. (1992) Wave Only	$\frac{S}{D} = 1.3(1 - \exp[-0.03(KC - 6)]); \quad KC \geq 6$
Sumer and Fredsøe (2001) Wave and Current	$\frac{S}{D} = \frac{S_c}{D}(1 - \exp[-\mathrm{A}(KC - \mathrm{B})]); \quad KC \geq 4$

Note: y_s = depth of scour; b = pile width; y_o = depth of flow around the pile; ϕ = shape coefficient; Fr_1 = upstream Froude number; b_e = projected width of the pier normal to the flow (m); D_{50} = particle size that is 50% finer than the bed material (m); K_1 = correction factor for pier shape; K_2 = correction factor for angle of attack of flow; K_3 = correction factor for bed condition; K_4 = correction factor for bed armoring; S = equilibrium scour depth (m); D = pile diameter (m); S_c = scour depth associated with the current only condition; and A and B = parameters related to the combined orbital velocity and current velocity.

but would have introduced further uncertainties in their requirement of additional unknown input parameters.

Soil samples were collected by hand from the Mexico Beach, FL, area. The grain-size distribution and specific gravity of the Mexico Beach, FL, sand was determined following ASTM D6913 (ASTM 2017a) and ASTM D854-14 (ASTM 2014), respectively. Following ASTM D6913 (ASTM 2017a), the sand was sieved through sieve numbers 4, 10, 20, 40, 100, and 200. The specific gravity of the Mexico Beach, FL, soil was determined using a KIMAX 28015 250 mL volumetric flask in accordance with ASTM D854-14 (ASTM 2014).

The specific hydrodynamic conditions that caused the measured scour depth at the 30 pile locations are unknown and an estimated range was created using two sources: an in situ USGS gage located at the pier [the pier is visible in Fig. 3(a); for an image of the gage, please see Kennedy et al. 2020], providing water depth and wave height measurements, and high-water marks reported throughout the Mexico Beach, FL, area (Kennedy et al. 2020; USGS 2020). The USGS gage, FLBAY03283, reported a maximum surge peak of 5.16 m NAVD88 and maximum wave crest elevation of 6.28 m NAVD88 (Kennedy et al. 2020). The gage reported a maximum significant wave height of 2 m in approximately 3 m of water above the ground surface (Kennedy et al. 2020). The evolution of inundation depth versus time and the wave height versus time retrieved from the wave gage can be found in Kennedy et al. (2020). The sampling frequency (0.03 Hz) of this gage prevented the collection of wave frequency information (Kennedy et al. 2020). The high-water marks reported a range of water depths above ground level from 0.6 to 3.5 m (USGS 2020). For scour prediction purposes, the range of wave heights was extended from the 2 m reported by the in situ gage to 80% of the water depth to account for waves larger than reported (e.g., a maximum of 2.8 m wave height instead of 2 m in 3.5 m water depth). The maximum water depth used for the equations was the maximum above ground

Table 3. Comparison of input parameters used in this study and the conditions of the respective studies for which the equations were developed

Input parameter	This study	Froehlich (1988)	FHWA (2012)	Sumer et al. (1992)	Sumer and Fredsøe (2001)
Water depth (m)	0.1–3.5 (0.34–12.1)	0.6–19.5 (0.06–2.0)	0.1–0.55 (0.5–2.75)	0.4 (3.8)	0.4 (2)
Median grain size (mm)	0.25–0.31	0.008–90	0.24–5.35	0.18–0.58	0.2
Wave height (m)	0.08–2.8 (0.28–9.7)	—	—	—	—
Wave period (s)	1–30	—	—	1.2–4.5	2.5–3.3
Keulegan–Carpenter number	0.94–233	—	—	4.4–102	4–26
Pile diameter (m)	0.2–0.46	0.29–19.5	0.05–0.35	0.01–0.2	0.3–0.9
Flow velocity (m/s)	0.5–5.9	0.15–3.6	0.25–0.8	—	0–0.84
Orbital velocity (m/s)	0.05–2.3	—	—	0.11–0.53	0.16–0.24
Pile shape (s)	Square, round	Square, round, sharp nosed	Square, round, other	Round	Round

Note: For comparison, nondimensionalized (divided by average pile width) forms of water depth and wave height (where applicable) are found in parenthesis below the respective parameter.

water depth reported from high-water marks (i.e., 3.5 m) (USGS 2020). The minimum water depth was chosen as 0.1 m to represent the early stages of inundation and to correspond with the minimum water depth from FHWA (2012).

From Dean and Dalrymple (1991), estimations of the breaker depth were made using the maximum significant wave height reported by the gage (i.e., 2 m) in a maximum water depth of 3.5 m and estimated slope of 0.54% across the streets of Mexico Beach, FL. With a breaker index of 0.82 ($a = 4.25$, $b = 0.82$), the necessary depth of water to induce breaking of the 2 m waves is 2.4 m. This implies that the reported waves with 2 m significant height in the 3.5 m water were not breaking. However, individual waves would have been larger than 2 m, and there is additional uncertainty as both water depths and wave heights were changing rapidly with time (~3 h) and throughout the Mexico Beach, FL, area (Kennedy et al. 2020). Therefore, the role of wave breaking on the observed scour development cannot be excluded from the available data and was not captured by the prediction equations used. The effects of breaking waves were considered independently from nonbreaking waves via the studies performed by Bijker and De Bruyn (1988), Carreiras et al. (2000), and Nielsen et al. (2012) and can be found in the "Discussion" section.

Since in situ measurements of wave period or flow velocities during Hurricane Michael in the Mexico Beach, FL, area have not been recorded by any source known to the authors, these parameters were estimated. Young (2003) provided a method to estimate the peak wave period generated by a hurricane as a function of surface wind speeds measured at landfall (71.5 m/s, 139 kt) and significant wave height (2 m) (Beven et al. 2019; Kennedy et al. 2020). From this approximation, the peak period of waves generated by Hurricane Michael was around 14.6 s. The ordinary gravity wave classification of wave periods (1–30 s) was used, as it incorporated the peak period estimation and provided a range of wave periods to be tested (Munk 1950). For maximum current velocity, a shallow water relationship was assumed (i.e., the square root of the water depth times gravity) (Dean and Dalrymple 1991). From this relationship and a maximum water depth of 3.5 m, the maximum current velocity used was 5.9 m/s. The range of values used for the Sumer et al. (1992), HEC-18 (FHWA 2012), Froehlich (1988), and Froehlich Design (1988) equation can be found in Tables 3, 4, and 5.

Sensitivity Analysis

To quantify the effects of the range of input parameters on the predicted scour depths, a sensitivity analysis was performed. Instead of testing the range of each varied parameter at the same time, the scour depths were calculated by changing only one variable at a time to determine the effect the range of each parameter had on the predicted scour depth. When a variable was not tested it was held at a constant value representing the mean of the input parameter's range. The only input parameter that was not tested was the wave height, which was left as 80% of the water depth. The percent difference was determined as the difference between the maximum and minimum values divided by the maximum value. The ranges tested correspond with those given in Tables 3, 4, and 5, and the results are presented in Table 6.

Table 4. Input parameter ranges used for the Sumer et al. (1992) and the Sumer and Fredsøe (2001) scour prediction equations for this study

Input parameter	Range
Water depth (m)	0.1–3.5
Wave period (s)	1–30
Wavelength (m)	1–117
Wave height (m)	0.08–2.8
Wave number (m^{-1})	0.04–6.7
Orbital velocity (m/s)	0.05–2.3
Keulegan–Carpenter number	0.94–233

Table 5. Input parameter ranges for the HEC-18 (FHWA 2012), Froehlich (1988), and Froehlich Design (1988) equations for this study

Input parameters	Range
Water depth (m)	0.1–3.5
Water velocity (m/s)	0.5–5.9
L/a	1
Angle of attack (°)	0
Fr	0.09–5.96
Angle correction	1
Dune height correction	1.1
Grain size, d_{50} (mm)	0.25–0.31

Note: L = length of the pile (m); a = width of the pile (m); and Fr = Froude number.

Laboratory Liquefaction Tests

Simple laboratory liquefaction tests were designed to determine the necessary excess pore-pressure gradients required to liquefy the soils found in the Mexico Beach, FL, area. Tests were performed using a modified constant head hydraulic permeameter (Fig. 5). A funnel connected to a faucet was used to supply the permeameter with a constant head of water. The pressure gradient provided by the constant head forces the water to flow upward through the porous media. If the difference in pressure between the bottom and the top of the soil sample was large enough to overcome the effective weight of the soil, the soil would liquefy. A 0.05-kg weight was placed on the soil prior to each test; this served as an indicator of liquefaction. If the soil liquefied, the weight would sink to the

Table 6. Sensitivity analysis of input variables

	Equations, output range (percent difference)				
Input parameter	Range (constant)	Froehlich (1988) Wave and Current	Froehlich (1988) Design Wave and Current	HEC-18 (FHWA 2012) Wave and Current	Sumer et al. (1992) Wave Only
Water depth (m)	0.1:0.01:3.5 (1.8)	0.167–0.599 (72%)	0.497–0.930 (47%)	0.792–1.28 (38%)	0.135–0.409 (67%)
Median grain size (mm)	0.25:0.001:0.31 (0.28)	0.468–0.476 (1.7%)	0.798–0.806 (1%)	N/A	N/A
Wave period (s)	1:0.01:30 (15.5)	0.000–0.472 (100%)	0.00–0.802 (100%)	0.00–1.17 (100%)	0–0.424 (100%)
Pile diameter (m)	0.20:0.01:0.46 (0.33)	0.346–0.580 (40%)	0.546–1.04 (47%)	0.844–1.45 (42%)	0.254–0.466 (45%)
Flow velocity	0.5:0.01:5.9 (3.2)	0.316–0.533 (41%)	0.636–0.863 (26%)	0.511–1.521 (66%)	N/A
Shape Factor	1 or 1.1 (1)	0.418–0.460 (9%)	0.748–0.790 (5%)	N/A	N/A

Note: Percent differences are shown in parentheses.

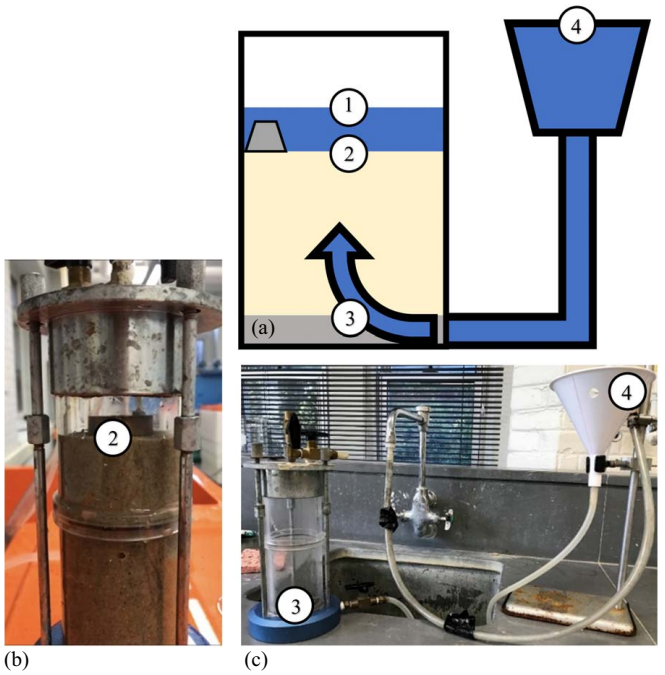

Fig. 5. (Color) Laboratory liquefaction test: (a) A conceptual sketch of the laboratory liquefaction test setup showing the direction of flow (blue arrow), constant head source (blue trapezoid), soil media (beige rectangle), porous stone (gray rectangle), and mass used to indicate liquefaction (gray trapezoid); (b) The apparatus was prepared with a soil sample and a weight placed on the soil. Since the soil has not been liquefied it can support the 50 g mass; and (c) The apparatus connected to the funnel and faucet, which supply the constant head.

bottom of the apparatus [similar to Fig. 1(c)]. When this occurred, the tubing connecting the funnel to the apparatus was closed. This allowed for the pressure difference between the bottom and top layers of the sand to be calculated with the Bernoulli equation [Eq. (1)] under the assumption that there is a sufficiently small (or no) difference in the velocity components and no head loss.

$$\frac{p_1}{\gamma} + z_1 = \frac{p_2}{\gamma} + z_2 \tag{1}$$

where p/γ = pressure head of a point of interest (m) with p being equal to the pressure at the point (kPa) and γ being the specific gravity of water (kN/m^3); and z = elevation of a point of interest from a datum (m).

For a fluid of known specific weight, the pressure head related to the fluid is equal to the pressure exerted by the fluid divided by its specific weight. This relationship, combined with the assumption that the specific weight of seawater is a constant 10.1 kN/m^3, allows for the terms of pressure and pressure head to be used interchangeably within this paper. Similarly, the pressure gradient and the pressure head gradient are both the difference in pressure or pressure head at two different locations and are used interchangeably.

Table 7. Geotechnical properties of prepared soil samples for liquefaction tests

	Parameter				
Site	γ_d (kN/m^3)	e	n	w	S
Mexico Beach	13.9–15.3	0.72–0.89	0.42–0.47	0.23–0.26	0.69–0.90

Note: γ_d = sample's dry unit weight; e = void ratio; n = porosity; w = water content as a decimal; and S = saturation as a decimal.

Using Eq. (1) for two sets of locations (Points 1 and 2 and Points 3 and 4 in Fig. 5, respectively), the pressure head can be found just above and below the sand column. When solving Eq. (1) for both sets of locations, the velocity head is assumed to be either the same at each location or small enough that it can be ignored, leaving the water elevation as the only variable. Since the parameters used to solve Eq. (1) are taken during the moment of liquefaction, the resulting pressure head is assumed to represent the liquefaction pressure for that given trial of the experiment.

In order to determine what pressure gradients would liquefy the soil of specific conditions, the soil samples collected from the Mexico Beach, FL, area were prepared for the liquefaction tests using a soil raining device as described in Eid (1987). The dry unit weight (γ_{dry}) in kN/m^3, void ratio (e), porosity (n), water content (W), and saturation (S) values were calculated to provide context to possible in situ conditions. The dry unit weight, void ratio, and porosity values fell within normal ranges for sand (Lambe and Whitman 1969); these values can be found in Table 7. Eqs. (2)–(6) were used to calculate the respective parameters presented in Table 7.

$$\gamma_{dry} = \frac{W_T}{\forall} \tag{2}$$

$$e = \frac{G_s \gamma_w}{\gamma_{dry}} - 1 \tag{3}$$

$$n = \frac{e}{e+1} \tag{4}$$

$$w = \frac{W_w}{W_s} \tag{5}$$

$$S = \frac{G_s w}{e} \tag{6}$$

where W_T = weight of the sand and water in the sample (kN); $\forall$ = volume of the sample (m^3); G_s = specific gravity of the soil

(unitless); γ_w = unit weight of water (kN/m^3); W_W = weight of the water in the sample (kN); and W_S = weight of the sand in the sample (kN). Further information on Eqs. (2)–(6) can be found in geotechnical textbooks such as Lambe and Whitman (1969).

To simulate in situ sediment conditions, the soil was first rained into the hydraulic permeameter (as described in Eid 1987) and then weighed. Second, the permeameter was slowly filled with water until the water just reached the top of the sand. Then the permeameter, sand, and water were weighed again. The ranges of soil properties in the prepared laboratory samples yielded a range of liquefaction pressure head values. Minimum and maximum liquefaction excess pressure head values were used to provide comparison with the field data and the Mory et al. (2007) equation [Eq. (7)] to predict momentary liquefaction. These laboratory tests served the purpose of determining the pore-pressure gradients needed to initiate momentary liquefaction of the Mexico Beach, FL, sands.

The range of gas contents of the prepared samples (Table 7, 10%–31%) was substantially larger than the ∼5% reported by Mory et al. (2007). However, the sediments tested by Mory et al. (2007) were routinely subjected to tidal and wave forces. The sands examined in this study were 100–350 m from the shoreline shown in Fig. 2(d) and would not experience tidal or wave forcing except during extreme storm events. However, rainfall from Hurricane Michael would be expected to increase the moisture content of the sediment. Both Yang and Davidson-Arnott (2005) and Paprocki et al. (2021) noted an increase of moisture content ranging from 4% to 25% depending on local site conditions, albeit from nonhurricane-induced rainfall. Rainfall in Mexico Beach, FL, may have been more intense than the conditions reported in these studies.

Thus, the moisture content of the normally dry sands [100–350 m from shoreline, Fig. 2(d)] could have increased to 25% or more prior to inundation, depending on the intensity of the rainfall and sediment bulk density (a looser sediment generally drains quicker reducing moisture content, Lambe and Whitman 1969). The moisture content of a sediment can be related to the degree of saturation (the volume of water within a sediment sample) through a simple equation (e.g., Lambe and Whitman 1969). Using the average sediment properties given in Table 7, as well as the specific gravity of the sediment (see the "Results" section), a moisture content of 25% corresponded to a degree of saturation of 86% (and a gas content of 14%). It is possible that the degree of saturation was larger than this value, depending on the intensity of the rainfall and local sediment properties (i.e., sediment bulk density and drainage). However, Mory et al. (2007) state that as little as ∼5% gas content is needed to significantly increase the risk of momentary liquefaction. Onshore sediments may therefore be at an increased risk of liquefaction due to their normally drier state compared with offshore or riverine sediments.

Liquefaction Prediction after Mory et al. (2007)

The liquefaction pressure equation [Eq. (7)] detailed in Mory et al. (2007) was used to provide another assessment of likelihood of liquefaction. Eq. (7) provides an estimate of the required pressure head gradient to liquefy a soil layer,

$$\frac{\Delta P_{2,1}}{\rho_f g} = h\left[\left(\frac{\rho_s}{\rho_f}\right)(1-n) + n - (n)C_{\text{gas}}\left(1 - \frac{\rho_g}{\rho_f}\right)\right] \tag{7}$$

where $\Delta P_{2,1}/\rho_f g$ = difference in excess pressure head between two layers of soil with Position 2 being below Position 1 (m); $\rho_{(f,\,s,\,g)}$ = density of the fluid (f), soil (s), or gas (g), respectively (kg/m^3); C_{gas} = amount of gas within the soil (decimal); and h = height of soil layer being liquefied (m).

The porosity and gas content of the soil are required to solve Eq. (7); however, these in situ values were not known for the Mexico Beach, FL, sand. Therefore, a range of porosities (0.25–0.47) and gas contents (0%–31%) were used to generate multiple liquefying excess pressure head values from Eq. (7), which encompassed the minimum and maximum sediment values obtained in the laboratory tests. The minimum and maximum liquefying excess pressure head values were then compared with laboratory liquefying excess pressure head results. If the laboratory liquefaction values and the Eq. (7) results were in agreement, then Eq. (7) could be used to predict what excess pressure head values could have caused liquefaction for the same sediment in different conditions (i.e., Hurricane Michael).

Field Measurements in Yakutat, AK

With the laboratory liquefaction pressure head and the theoretical liquefaction excess pore-pressure head values obtained from Eq. (7), it became necessary to determine whether these excess pore-pressure heads would be feasible in the field. As no pressure sensors were buried in the locations of interest in Mexico Beach, FL, before the hurricane, data were taken from two pore-pressure sensors deployed in the intertidal zone at Cannon Beach in Yakutat, AK, United States. These pressure sensors were attached to a vertical bar similar to previous experiments (e.g., Raubenheimer et al. 1998; Mory et al. 2007; Michallet et al. 2009; Guest and Hay 2017; Florence and Stark 2019). The intertidal zone was chosen at Cannon Beach, AK, as it becomes subaqueous during high tide and subaerial during low tide with water depths ranging from 0 m (at low tide, sensors are not submerged) to 1.3 m water depth. The assumption was made that this would exhibit similar processes to the normally subaerial conditions at Mexico Beach, FL, being suddenly inundated during Hurricane Michael and was similar to the conditions in Mory et al.'s (2007) study. Sediments at Cannon Beach, AK, are predominantly silica sands with a median grain size of 0.31–0.39 mm (Albatal et al. 2020). It should be noted that the maximum water depth (1.3 m) and significant wave height (0.83 m) at Cannon Beach, AK, at high tide are 37% and 42% of the maximum above ground surface high-water mark (3.5 m) and significant wave height (2 m) reported at Mexico Beach, FL (Kennedy et al. 2020; USGS 2020). Sediment grain-size distributions are similar between the two sites and are discussed later.

An excess pore-pressure time series was recorded inside the soil media at two different vertical locations by a pair of *RBRsolo*^{3} pressure sensors at Cannon Beach, AK. The locations of these sensors in the soil were similar to Locations 2 and 3 in the laboratory experiments (Fig. 5): the topmost pressure sensor was at the interface between the seabed and the seawater. The second sensor was 10 cm below the topmost sensor. The excess pore-pressure data were filtered to remove waves outside of the ordinary gravity waves, as defined by Munk (1950), leaving the wave period range used in the prediction equations (Table 3) as well as the theoretical peak wave period (14.6 s) generated by the hurricane from Young (2003). The field excess pressure head gradients under normal wave conditions (e.g., no storm was present, significant wave height of 0.83 m) were evaluated and then compared with the pressure head gradients given by the laboratory experiments and Eq. (7). The excess pressure head gradient was calculated by subtracting the excess pressure head values recorded by the sensor at the bed surface (Fig. 5, Position 2) from the excess pressure head values recorded by the sensor buried within the sediment (Fig. 5, Position 3) (Mory et al. 2007).

The data gathered from Yakutat, AK, were used to determine whether the pressure head gradients from the laboratory liquefaction tests and Eq. (7) could occur in the field. Should the pressure head gradients measured at Cannon Beach, AK, meet or exceed the liquefying pressure gradients from the laboratory tests or Eq. (7), it is likely that Mexico Beach, FL, sediments would liquefy under similar wave conditions as those in Yakutat, AK, and even more so during hurricane conditions.

Pressure Attenuation

Wave attenuation through the soil media was predicted using Yamamoto et al.'s (1978) model. This analytical model predicts the excess pore-pressure attenuation response in the soil as a function of both wave and geotechnical characteristics. The model is used to determine the excess pore-pressure head values at the bed surface and then at some user-given depth within the sediment as a function of wave frequency. The excess pressure with time field data are then converted into the frequency domain using the fast Fourier transform (FFT) algorithm. The frequency domain excess pressure signal from within the sediment media is then divided by the frequency domain excess pressure signal at the bed surface, which is then compared with the Yamamoto et al. (1978) model.

The Yamamoto et al. (1978) model can also be used to observe the changes in excess pore-pressure attenuation as a result of different sediment properties (e.g., permeability) of two soil samples (i.e., the Cannon Beach, AK, and the Mexico Beach, FL, sands). An excess pore-pressure attenuation model of a sediment described by the Yamamoto et al. (1978) model that displays significant attenuation of excess pore pressures may indicate the possibility of increased liquefaction risk compared with a sediment that exhibits minimal excess pore-pressure attenuation. This is because the attenuation of the excess pore-pressure signal in the trough phase as sediment depth increases leads to larger magnitudes of upward-directed excess pore-pressure gradients (by nature of less negative excess pore pressures with depth during the trough) and thus an increased likelihood of momentary liquefaction (Mory et al. 2007).

These methods sought to compare storm-induced field-measured scour holes against common prediction equations using a range of values, since the exact scour-inducing conditions were unknown. The source of discrepancy of underprediction was then discussed with a focus on momentary liquefaction, which was further investigated using laboratory and nonstorm conditions field data. Overprediction was not a focus of this study as this is preferred (safer) over underprediction of sediments.

Results

Scour Observations and Predictions

Fig. 6 shows the grain-size distributions for the sediment samples retrieved by hand from Mexico Beach, FL, during the reconnaissance mission and the soil samples at Cannon Beach, AK, in Yakutat, AK, used for the laboratory liquefaction experiments. The median grain size, d_{50}, of the Mexico Beach, FL, and Cannon Beach, AK, sands were 0.26 and 0.31 mm, respectively. With a coefficient of uniformity (C_u) and coefficient of curvature (C_c) of approximately 1.5 and 1.0, respectively, the Mexico Beach, FL, sand was classified as a poorly graded sand (SP) under ASTM D2487-17 (ASTM 2017b). Similarly, the Cannon Beach, AK sand has a C_u and C_c of approximately 2.2 and 1, respectively, classifying it as a poorly graded sand (SP) under ASTM D2487-17 (ASTM 2017b). Following ASTM D854-14 (ASTM 2014), the specific

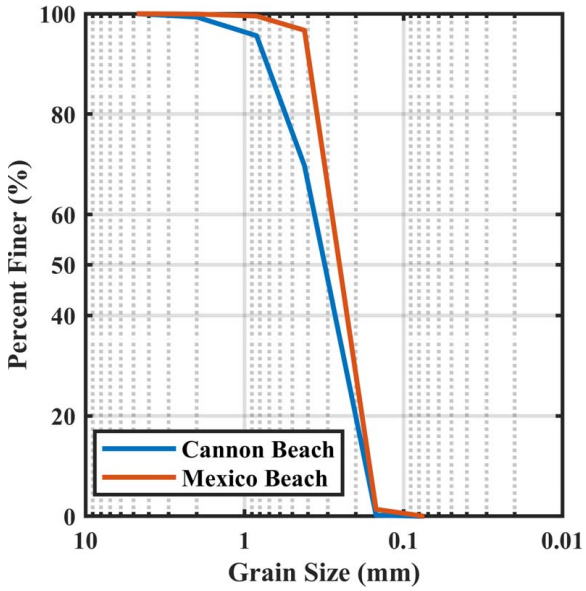

Fig. 6. (Color) Grain-size distributions for the Cannon Beach, AK and Mexico Beach, FL sands. Both soils are classified as a poorly graded sand (SP) after ASTM D2487-17.

gravity of the Mexico Beach, FL, and Cannon Beach, AK, sand were determined to be 2.67 and 2.92, respectively. The specific gravity of the Mexico Beach, FL, sand was at the upper limit of expected ranges for a sand. However, the specific gravity of the Cannon Beach, AK, sand was significantly higher than expected; this may be due to the mineral composition of the sand (i.e., heavy minerals) (Lane 1987). For the purpose of this study, the sands at these two sites could be considered similar.

Figs. 7–10 were created using the information in Tables 1, 2, 4, and 5 to show a comparison of the scour depths predicted by the equations in Table 2 and the scour depths measured in the field. The range of input parameters from Tables 4 and 5 were used in the first four equations in Table 2. Linearly spaced arrays consisting of 30 points each were used for median grain size, water depth, wave period, flow velocity, and wave height. Parameters such as wavelength, Froude number, orbital velocity, and KC number were then calculated using each combination of the respective parameters. Wave parameter combinations that induced breaking due to depth or steepness limitations were not used. The scour depth values from the three current only scour equations (the first three equations in Table 2) were then used in the Sumer and Fredsøe (2001) equation as S_c. For example, Fig. 9 was created by using the scour depths (y_s) given by the Froehlich (1988) equation as the scour depth from currents (S_c) in the Sumer and Fredsøe (2001) Wave and Current equation. This allowed for the Froehlich (1988) current only equation to also account for the effects of waves through the Sumer and Fredsøe (2001) modification, thus, being called the "Froehlich Wave and Current" equation to represent this combination. This process was repeated for each of the current only equations yielding Figs. 8–10. The Sumer et al. (1992) equation (Fig. 10), being a wave only equation, comprises only this equation.

The end result of this process was a decrease in the lower bounds of each equation's prediction range. This process is demonstrated where the low wave period (1–5 s) scour predictions are shown in blue to the left of the black current only Froehlich (1988) data points is for Fig. 9. The full range of the Sumer and Fredsøe (2001) modification is not shown as the maximum scour

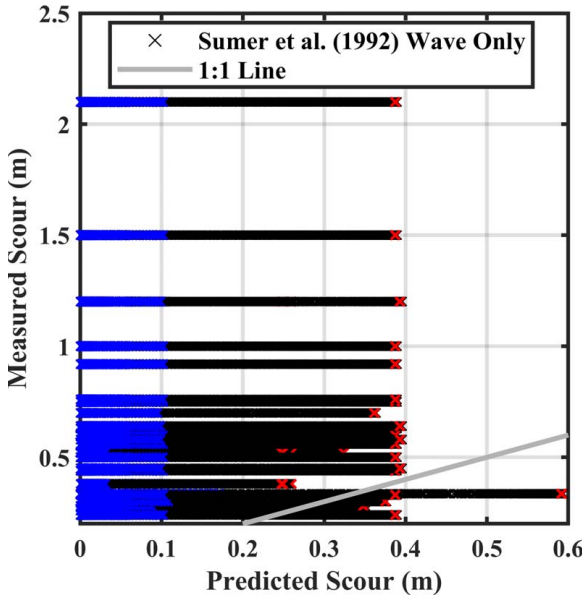

Fig. 7. (Color) Comparison of Sumer et al. (1992) scour prediction equation from wave only conditions. Points falling on the diagonal 1:1 line indicate that the predicted scour is equal to the measured scour depth. Each horizontal group of points represents one of the 30 measured scour depths. Red data points denote predictions with a water depth of 3.5 m and wave height of 2 m, blue denote wave periods between 1–5 s, and black denote wave periods between 6–30 s.

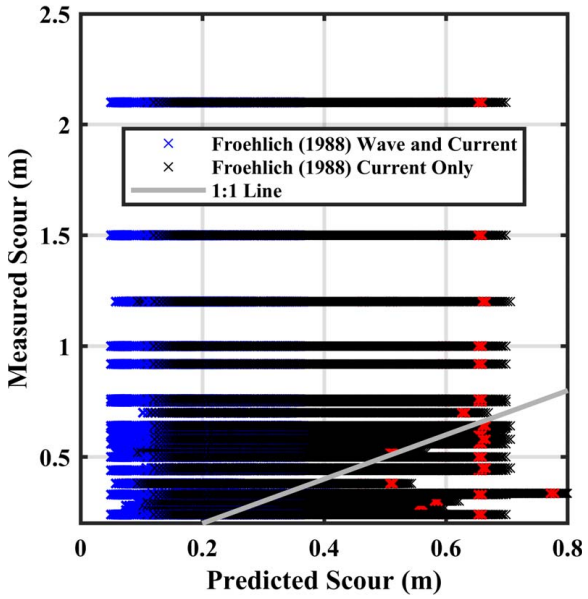

Fig. 9. (Color) Comparison of the Froehlich (1988) and the Sumer and Fredsøe (2001) Wave and Current scour prediction equations and the measured scour. Points falling on the diagonal 1:1 line indicate that the predicted scour is equal to the measured scour depth. Each horizontal group of points represents one of the 30 measured scour depths. Red data points denote predictions with a water depth of 3.5 m and wave height of 2 m. Here blue data points are the scour depth prediction values from the combination of the Froehlich (1988) and Sumer and Fredsøe (2001) prediction equations, while the black data points are the scour depth prediction values from only the Froehlich (1988) prediction equation.

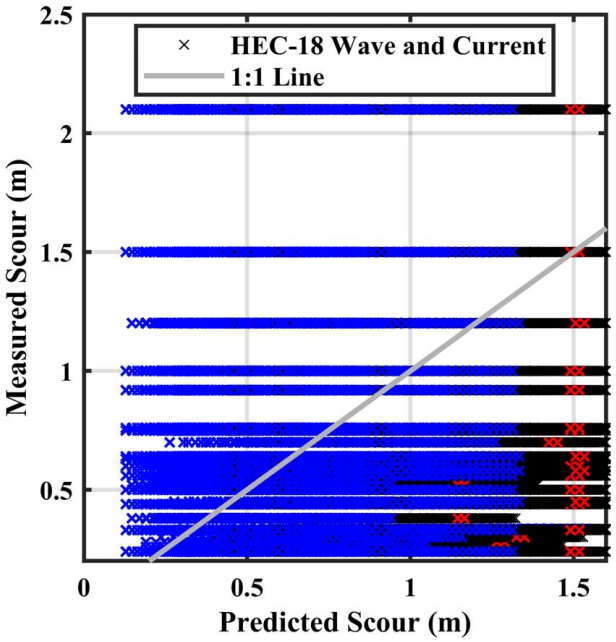

Fig. 8. (Color) Comparison of the HEC-18 (FHWA 2012) and the Sumer and Fredsøe (2001) Wave and Current scour prediction equations and the measured scour. Points falling on the diagonal 1:1 line indicate that the predicted scour is equal to the measured scour depth. Each horizontal group of points represents one of the 30 measured scour depths. Red data points denote predictions with a water depth of 3.5 m and wave height of 2 m, blue denote wave periods between 1–5 s, and black denote wave periods between 6–30 s.

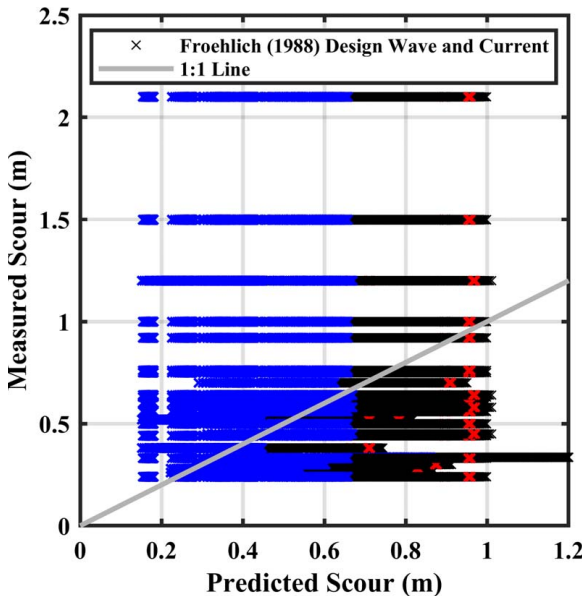

Fig. 10. (Color) Comparison of the Froehlich Design (1988) and the Sumer and Fredsøe (2001) Wave and Current scour prediction equations against the field measured scour. Points falling on the diagonal 1:1 line indicate that the predicted scour is equal to the measured scour depth. Each horizontal group of points represents one of the 30 measured scour depths. Red data points denote predictions with a water depth of 3.5 m and wave height of 2 m, blue denote wave periods between 1–5 s, and black denote wave periods between 6–30 s.

depth predicted is the same as the current only Froehlich (1988) results, which would have produced overlapping points.

Each horizontal group of data points in Figs. 7–10 represents the scour depth values calculated by each respective predictive equation for each field-measured scour depth. The range of input values (Tables 4 and 5) combined with the repeated or similar field-measured scour depths and pile dimensions (Table 1) caused overlap of calculated data points. This resulted in the appearance of fewer than 30 individual horizontal data groups. The red data points represent scour predictions with a water depth of 3.5 m and a significant wave height of 2 m. These points were highlighted as they represent the maximum in situ reported values and have the least amount of uncertainty associated with them. The blue data points correspond to scour depths predicted using a wave period between 1 and 5 s to highlight the difference in possible scour depth caused by wave periods within the prediction equations' tested limits (Table 3, Row 4, Columns 5 and 6) and the black data points with a wave period ranging from 6 to 30 s (i.e., ordinary gravity waves, Munk 1950).

As to be expected when dealing with prediction equations, unknown conditions, and complex processes, not all measured scour hole depths could be predicted by all prediction equations (i.e., were not on the gray 1:1 line). In most cases, this issue applied to deeper scour holes, resulting in underpredictions. Reasons for the inability to accurately predict the scour hole depths include, but are not limited to, complex or different flow geometry from that accounted for in the equations (e.g., flow no longer around a slender pile due to debris), uncertainty in the conditions that caused the scour (however, it should be noted that a wide range of feasible conditions was tested), and scour processes that were not accounted for in the equations, such as rapid inundation events, high-velocity return flows, breaking waves, momentary liquefaction, refilling of the scour holes, and others not explicitly discussed here.

The overprediction of these equations may be related to the range of parameters (specifically, wave period and flow velocity) used that encompassed values larger than what truly occurred and the conservative nature of the equations tending toward overprediction (FHWA 2005; Falcone and Stark 2016). However, the underprediction resulting from these equations is of interest, as the range of input values given for each of these equations was meant to represent all combinations of the feasible parameters that could actually have occurred. Additionally, these equations are in general meant to represent a conservative estimate, that is, to overpredict (FHWA 2005; Falcone and Stark 2016). Therefore, underprediction presents a concern. Possible sources of underprediction are numerous and are discussed more in the section "Scour Equations"; however, from previous studies, momentary liquefaction can be hypothesized to be a scour-enhancing process, as outlined in the "Introduction".

Sensitivity Analysis

The results of the sensitivity analysis are given in Table 6. Percent differences are shown in parenthesis next to the range of output values for each equation. Equations that experienced no change in their prediction values as a result of not having a specific parameter (e.g., median grain size for non-Froehlich 1988 equations) were labeled with "N/A." Of the parameters tested, wave period had the most significant impact on the predicted scour range (mean of 100% percent difference). This is a byproduct of each current only scour equation being fed into the Sumer and Fredsøe (2001) Wave and Current scour equation. The Sumer and Fredsøe (2001) equation extends the lower limit of the predicted scour depths by including the effects of wave-induced scour. It has been shown that wave-based scour, in general, causes less scour than current only scour (Sumer and Fredsøe 2001). Thus, the variation in the wave period explains the extension of the lower limit of predicted values but has no effect on the maximums and does not explain underprediction.

The wave period range was determined by calculating the theoretical peak wave period generated by Hurricane Michael from Young (2003) and then choosing the category that the peak period (~14.6 s) fell into by Munk (1950) (i.e., 1–30 s, ordinary gravity waves). To the authors' knowledge, there are no in situ measurements of the wave period caused by Hurricane Michael at Mexico Beach, FL. The gage at Mexico Beach, FL, FLBAY03283, did not have a sufficient sampling period to capture wave period data (30 s sampling period, Kennedy et al. 2020).

Water depth had the second highest mean percent difference of 56%, with pile diameter and flow velocity having the same average percent difference of 44%. Water depth measurements were taken from in situ measurements of high-water marks from the Mexico Beach, FL, area (USGS 2020). However, as stated by Kennedy et al. (2020), the water depth measurements presented here could have been exceeded, introducing additional uncertainties. Pile diameters were measured in the field at each location that the scour depths were measured. Flow velocity measurements were not available from in situ measurements. The maximum flow velocity (5.9 m/s) was calculated using the shallow water wave relationship with a maximum depth of 3.5 m. Shape factor and median grain size had mean percent differences of 7% and 1%, respectively. These represent the lowest mean percent errors of all the input parameters tested and are measured values.

Pore Pressures and Momentary Liquefaction

The excess pore-pressure head field data taken from Cannon Beach, Yakutat, AK, were compared with the laboratory liquefaction pore-pressure head results and the liquefaction pore-pressure head determined by Eq. (7) (Figs. 11 and 12). For both figures, the liquefaction criteria from the laboratory tests was determined from the Mexico Beach, FL, sands for a soil depth of 0.06 m. For Fig. 11, the liquefaction criteria for the Mory et al. (2007) equation [Eq. (7)] was determined using this same sediment depth and specific gravity of the Mexico Beach, FL sand (0.06 m and 2.67, respectively). Therefore, the horizontal lines in Fig. 11 are both derived from Mexico Beach, FL, sediment values. However, textural properties of the sediments from Mexico Beach, FL and Cannon Beach, AK, are similar; therefore, it may be argued that similar pore-pressure gradients would develop under similar conditions between the two sites.

For Fig. 12, the liquefaction criteria for the Mory et al. (2007) equation was determined using a soil depth of 0.1 m and specific gravity of 2.92, to match the field conditions at Cannon Beach, AK. Therefore, the top two horizontal lines in Fig. 12 represent the Mory et al. (2007) equation [Eq. (7)] using the Cannon Beach, AK, sediment depth (0.1 m) and specific gravity (2.92), while the bottom two horizontal lines are from the laboratory test (Mexico Beach, FL, sand, 0.06-m depth, specific gravity of 2.67).

In this matter, it was tested whether moderate wave action (significant wave height of 0.58–0.83 m and water depth of 0.63–1.3 m for the ebb and high tide, respectively) in the field could create vertical pressure gradients sufficient to achieve liquefaction as determined in the laboratory tests and from Eq. (7). The laboratory tests yielded a potential liquefaction range for the Mexico Beach, FL, sediments of 0.14–0.17 m of excess pore-pressure head difference for a sediment depth of 0.06 m. The Mory et al. (2007) equation yielded a range of 0.11–0.12 m of excess pore-pressure head difference for the Mexico

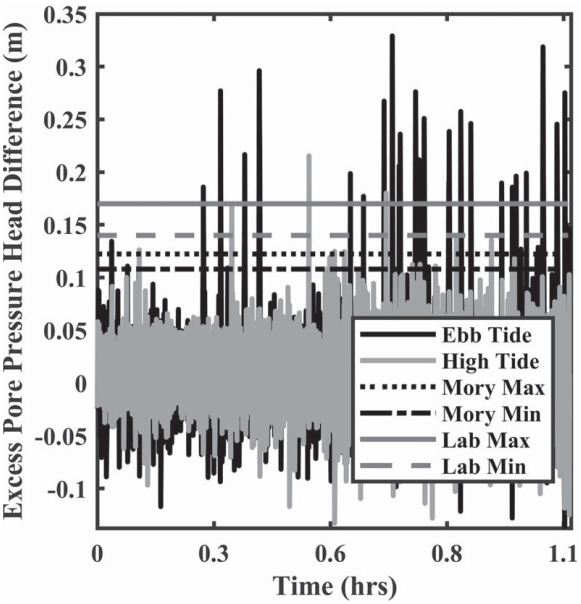

Fig. 11. Comparison of pressure difference between bed surface and buried sensor (~0.1 m separation) measured in the field (Cannon Beach, AK) during high- and ebb tide and liquefying excess pressure head difference determined in the laboratory experiments and Eq. (7) using the Mexico Beach, FL sands. When the field excess pore-pressure head difference (vertical lines) exceeds liquefaction criteria (horizontal lines), liquefaction is likely to occur. Liquefaction criteria for the Mory et al. (2007) equation were determined using the same soil depth and specific gravity Mexico Beach, FL, sand (~0.06 m, 2.67 respectively). The laboratory minimum and maximum exceeded the Mory et al. (2007) equation maximum value.

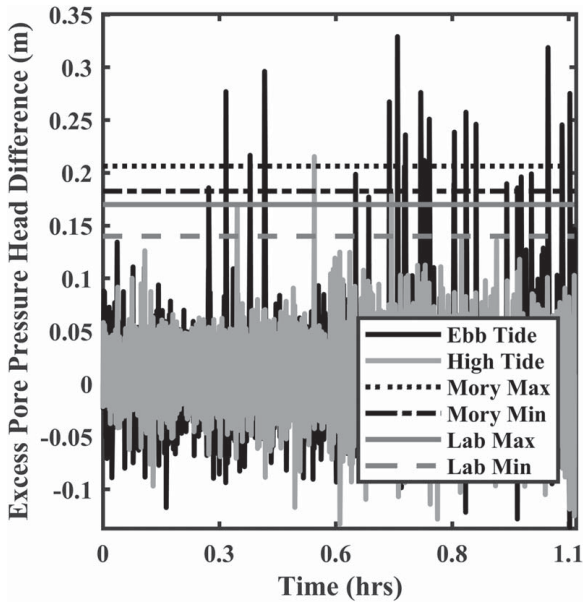

Fig. 12. Comparison of pressure difference between bed surface and buried sensor (~0.1 m separation) measured in the field (Cannon Beach, AK) during high and ebb tide and liquefying pressure head difference determined in the laboratory experiments and Eq. (7) using the Mexico Beach, FL, sands. When the field excess pore-pressure head difference (vertical lines) exceeds liquefaction criteria (horizontal lines), liquefaction is likely to occur. Liquefaction criteria for the Mory et al. (2007) equation were determined using the same soil depth and specific gravity as the field-collected excess pore-pressure measurements (~0.1 m, 2.92, respectively). The Mory et al. (2007) minimum and maximum exceeded the maximum laboratory value.

Beach, FL, sediment (Fig. 11). The differences between these range (21% difference for the minimum, 30% difference for the maximum) most likely arose from the small size of the permeameter (3.2 cm diameter) causing sediment–wall interactions. The Mory et al. (2007) values for Fig. 12 yielded a liquefaction range of excess pore-pressure head difference of 0.18–0.21 m, the differences from the laboratory tests were likely to have been caused by the differences in sediment depth (0.06 m versus 0.1 m) and the differences in specific gravity (2.67 versus 2.92).

In Figs. 11 and 12, the excess pore-pressure head difference (vertical lines, caused by wave propagation) is calculated as the difference between the excess pore-pressure head values recorded by the pressure sensors as mentioned previously (e.g., pressure head within the sediment media minus the pressure head recorded at the bed surface, at a distance of 0.1 m). The value of the excess pore-pressure head difference from the field data (black and gray, nonhorizontal lines) could fall into three distinct categories: (1) negative, (2) positive but less than Mory et al. (2007) [Eq. (7)] and/or laboratory values, or (3) greater than Mory et al. (2007) [Eq. (7)] and/or laboratory values.

(1) When the pressure head differences were negative, the pressure head recorded at the bed surface (Fig. 5, Position 2) was greater than the pressure head recorded below it (Fig. 5, Position 3). This means that the pressure gradient was directed downward from the bed surface to within the sediment media [Fig. 1(b)]. This additional force may increase the strength of the soil, reduce liquefaction risk, and is beyond the scope of this study.

(2) When the pressure head difference between the two positions was positive but less than the liquefaction pressure heads determined either from Eq. (7) or from the laboratory tests, the pressure gradient was directed from within the sediment (Fig. 5, Position 3) to the bed surface (Fig. 5, Position 2) [Fig. 1(c)]. This acts similar to a buoyancy force lifting the sediment particles and may increase erodibility. While these values may be important for scour risk assessment, they were not the focus of this study.

(3) When the excess pore-pressure head difference determined from the pressure sensors met or exceeded the liquefaction pressure head values, then the pressure head was large enough and directed in such a way as to cause the soil to liquefy (i.e., behave like a fluid rather than a granular solid) [Fig. 1(c)]. Pressure values in this range are the most critical as the shear stress required to mobilize or transport the sediment is significantly reduced (Shields 1936; Sakai et al. 1992; Mory et al. 2007). As can be seen from Figs. 11 and 12, both the high- and ebb tide at Cannon Beach in Yakutat, AK had instances when the laboratory liquefaction pressure head or the liquefaction pressure head determined from Eq. (7) were exceeded. Looking at the number of instances, the ebb tide (water depth of 0.63 m) showed more instances compared with the high tide (water depth of 1.3 m). This scenario may have an important role in sediment transportation and scour events and was the focus of this study.

Figs. 13 and 14 show the results of the frequency-dependent pressure signal attenuation caused by the wave pressure signal propagating vertically through the porous media, with Fig. 13 representing the ebb tide and Fig. 14 representing the high tide, as calculated from the Yamamoto et al. (1978) model. The solid blue line is created by taking the FFT of two pressure signals and dividing

the FFT of the bottom pressure sensor (P_2, located at Position 3 in Fig. 5) by the FFT of the topmost pressure sensor (P_1, Position 2 in Fig. 5) and then squaring. This ratio describes the amount of attenuation (or damping) of a pressure signal caused by a particular wave frequency. If there is no damping present in the bottom signal (P_2), the ratio approaches 1. In both Figs. 13 and 14, there is a discrepancy between the Yamamoto et al. (1978) model and the field data at very low frequencies. This was most likely caused by the removal of 0 Hz effects during data processing (e.g., removal of pressure caused by the still water depth and the atmosphere).

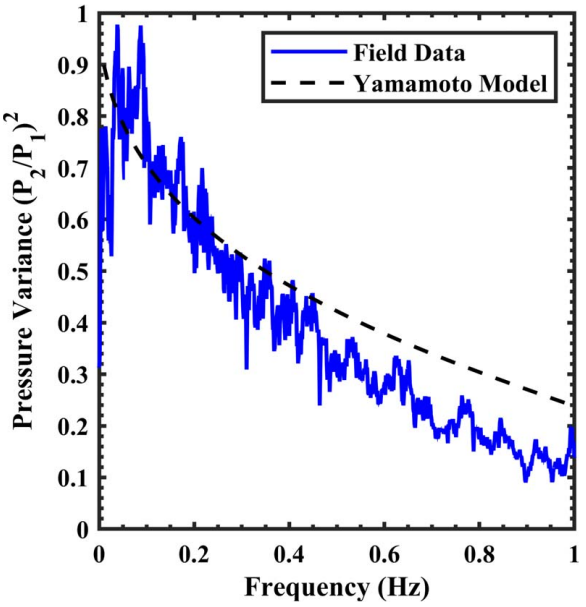

Fig. 13. (Color) Comparison of ebb tide field data and the Yamamoto et al. (1978) pressure dissipation model. Differences around 0 Hz were due to removal of 0 Hz influences (i.e., atmospheric and hydrostatic pressure).

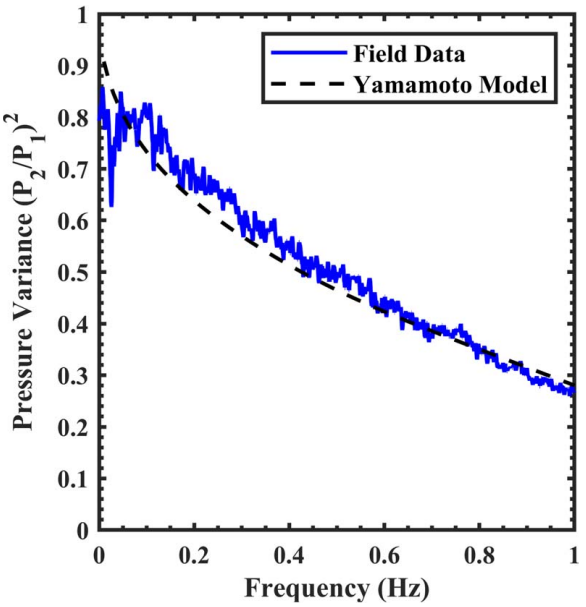

Fig. 14. (Color) Comparison of high tide field data and the Yamamoto et al. (1978) pressure dissipation model. Differences around 0 Hz were due to removal of 0 Hz influences (i.e., atmospheric and hydrostatic pressure).

The Yamamoto et al. (1978) model had greater difficulty predicting the pore-pressure response (i.e., greater discrepancies between the model and field data) during the ebb tide as compared with the high tide. In Fig. 13, the model seemed to predict the ebb tide pressure dissipation behavior well for frequencies of 0.10 to 0.22 Hz. There was some underprediction of the model from 0.04 to 0.10 Hz and overprediction for frequencies greater than 0.24 Hz. Conversely, there was greater agreement between the model and the field excess pore-pressure dissipation data across essentially all frequencies during high tide (Fig. 14). While the model underpredicted the pressure dissipation in the high tide from 0.10 to 0.60 Hz, the magnitude of the difference was less than that of the ebb tide. The cause of the differences in accuracy between the ebb- and high tides is currently unknown but may be linked to gas content and still water depth (Yamamoto et al. 1978; Mory et al. 2007). Figs. 13 and 14 show that the ebb tide may experience increased excess pore-pressure attenuation, which may result in larger or more frequent liquefaction inducing excess pore-pressure differences, as seen in Figs. 11 and 12.

Discussion

Scour Equations

Table 8 presents the number of prediction iterations that met or exceeded the 1:1 line in the respective Figs. 7–10 for each equation. This corresponds to a horizontal line from Figs. 7–10 meeting or being to the right of the 1:1 line. A number less than 15 indicates that more than half of the prediction attempts by that equation resulted in an underprediction. The input ranges used in each equation for Table 8, and whether the ranges tested here were within the ranges for each equation, can be found in Table 3.

The nature of these prediction equations is generally conservative and favors overprediction (FHWA 2005; Falcone and Stark 2016). By overpredicting the scour depth for a scenario, these equations have something similar to a built-in factor of safety. In this study, even the applied range of input parameters led to more accurate or even underpredicted scour hole depth estimates than would be expected from the conservative equations. Therefore, the specific effects of the Sumer and Fredsøe (2001) equation on the scour prediction range were not considered further since the equation does not correct underpredictions of current only cases (Fig. 9; blue points only extend the lower bound) and cannot be applied to wave only cases.

Sources of discrepancy between the prediction models and field measurements include, but are not limited to, limited inundation time, complex flow geometry, armoring effects, refilling of the scour hole from ex situ sediments, in situ conditions exceeding the range tested here, momentary liquefaction, scour caused by breaking waves, additional scour from flood water returning to the ocean, and the effects of debris (Sumer and Fredsøe 2002; Nielsen et al. 2012; Borga et al. 2017; Kennedy et al. 2020).

A limited inundation time should, in theory, cause an overprediction of the scour depth (Sumer and Fredsøe 2002). However, the focus of this study was the underprediction of the equations

Table 8. Instances of 1:1 line exceedance for each respective equation

Equation	Froehlich (1988)	Froehlich (1988) Design	HEC-18 (FHWA 2012)	Sumer et al. (1992)
Instances of 1:1 exceedance	21	23	28	6

that can be seen in Figs. 7–10. Complex flow geometry resulting from infrastructure and flow debris could result in disagreement between measurements and predictions. The effect of these two processes on scour depth is not accounted for in the equations or quantifiable from the available data. The refilling of scour holes from ex situ sediments would result in overpredictions by the scour equations as the measured depths become shallower.

The processes of armoring, winnowing, and the effects of grain-size distribution on the possible scour depth may also explain the under- and overprediction seen by the scour equations. However, the equations tested here do not account for any of these processes. Median grain size (d_{50}) is generally the only geotechnical parameter taken into consideration by scour equations. However, the median grain size was not sufficient to adequately describe sediments with different grain-size distributions, armoring, or an indicator of winnowing (Lambe and Whitman 1969). Additionally, the data collected for this study were not sufficient to draw conclusions on the possible impacts of armoring, winnowing, or grain-size distribution.

In situ conditions could have exceeded those used in this study, as discussed previously. The range of input parameters taken from in situ measurements attempted to prevent this; however, it is possible that these parameters varied greatly throughout Mexico Beach, FL, and some parameters did not have measurements. The measurements were performed during a rapid reconnaissance mission and did not include the placement of sensors during the hurricane by the authors. In the future, sensor deployments prior to hurricane arrival would be desired. However, the acquisition of, for example, all input parameters needed for this study during hurricane conditions would still be challenged by accurate prediction of inundation zones, structures at risk, equipment failure during storm conditions, and the risk of damage to equipment and to personnel associated with the deployment. Therefore, a reasonable range of input parameters was chosen to be applied to scour prediction equations that required only a limited number of additional assumptions on more complex input parameters in this study. For example, equations 3.12, 3.13, 3.22, 3.23 and others in Sumer and Fredsøe (2002) and equations in studies by Vanoni (2014) and Borga et al. (2017) would possibly prove more accurate, but they would add uncertainty in the form of additional parameters not seen in Table 2 (e.g., boundary layer thickness, consideration of armoring) in this study. While it is acknowledged that the ranges of input parameters (over accurate measurements) applied in this study prohibited the accurate prediction of a specific scour depth, it did indicate a risk for underprediction, representing an unfavorable risk for the respective structures. The reader is also referred to the sensitivity analysis.

Scour could have been deepened as flood water returned back to the ocean. This would have exacerbated any existing scour from intense return flow and would have caused underpredictions of the scour equations. Yeh and Mason (2014) studied the drawdown period of a tsunami and its effects on excess pore pressures and scour. They observed that severe scour can occur as a result of thin swift currents forming during the drawdown period eroding weak spots (Yeh and Mason 2014). Additionally, they found that during the drawdown period, momentary liquefaction occurred as a result of a rapid reduction of excess pore water pressure. This momentary liquefaction resulted in what Yeh and Mason (2014) termed "enhanced scour" (scour beyond what is expected from ordinary flows). However, no measurements on flood flows receding or excess pore pressures are available for the Mexico Beach, FL, area (Kennedy et al. 2020), and thus, no conclusions could be drawn on the impacts of the observed scour.

The analysis of scour equations thus far has ignored the role of breaking waves on the scour depth. While the calculations for breaker depth mentioned previously indicated that wave heights up to the significant wave height of 2 m in 3.5 m of water were not breaking, waves larger than this value or waves in different water depths would most likely have experienced breaking as wave height and water depth changed over the duration of the storm. Furthermore, the equations used for scour prediction did not take into consideration the difference in scour mechanisms due to breaking waves as compared with nonbreaking waves (Bijker and De Bruyn 1988; Carreiras et al. 2000; Nielsen et al. 2012). Nielsen et al. (2012) describe a particular distance between a pile and where a wave breaks that results in a significant scour depth. With the rapidly changing water depth and wave conditions during Hurricane Michael, coupled with the lack of in situ measurements of these parameters, it is possible that the piles used in this study experienced waves that broke at the distance described by Nielsen et al. (2012), leading to an increased scour depth.

Carreiras et al. (2000) and Nielsen et al. (2012) provide easy to use first approximations of scour depth as a function of pile diameter based on their laboratory experiments. Carreiras et al. (2000) reported a maximum scour depth equal to $1.04D$ and Nielsen et al. (2012) reported a maximum scour depth equal to $0.6D$. Comparing the pile diameters with the respective scour depth from Table 1, it can be seen that four piles (the bottom four with scour depths of 0.24, 0.26, 0.28, and 0.30 m) had a scour depth that ranged from $0.8D$ to $1.03D$. It is possible that breaking waves resulted in at least four scour depths listed in Table 1. Based on the data collected in this study and the two approximations provided by Carreiras et al. (2000) and Nielsen et al. (2012), it is unlikely that breaking waves alone explain all the observed underpredictions.

Momentary liquefaction from waves is another possible source of underprediction of the scour equations tested (Sakai et al. 1992; Mory et al. 2007; Yeh and Mason 2014; Stark 2017). The scour equations that accounted for wave interactions did not account for momentary liquefaction (Sumer and Fredsøe 2002). While without further testing it is difficult to say what accounts for the disagreement between predictions and measurements at the observed sites, the observed occurrences of underprediction are concerning and call for additional investigations. In this study, the possibility of momentary liquefaction enhancing scour was then further investigated based on laboratory testing and field recordings under no-storm conditions at a site with similar soil conditions.

Sensitivity Analysis

Of the parameters tested, wave period and flow velocity were the only parameters without any in situ measurements. Kennedy et al. (2020) indicated that reported high-water marks may be conservative and could have been exceeded during Hurricane Michael. This could be a source of underprediction, as a deeper water depth will yield larger scour holes from the equations used here. No in situ measurements of wave period were found, but an estimate was calculated as 14.6 s using Young (2003). The range of wave periods tested noticeably exceeds the wave periods tested in the Sumer et al. (1992) and Sumer and Fredsøe (2001) equations by a factor of ~10. The difficulty arises in the dichotomy between choosing a wave period within the ranges tested by the equations (1.2–4.5 s) or choosing a range that better represents the possible wave periods that the piles are exposed to in storm conditions (1–30 s, Munk 1950). Furthermore, the maximum current velocity (5.9 m/s) used for the predictive equation was an estimation based on a shallow water wave assumption as well as an assumption on the maximum water depth (3.5 m) (Dean and Dalrymple 1991).

As the water depth changes, assuming shallow water wave conditions persist, the maximum current velocity will also increase, according to the square root of water depth times gravity. It should also be noted that Matsutomi et al. (2011) proposed an additional constant to be multiplied to the shallow water relationship between velocity and water depth. This value ranges between 0.6 and 1.2 depending on the difference in water depth at the front and back of an inundated structure. While Matsutomi et al. (2011) studied the effects of a tsunami, not a hurricane, inundating a structure larger than a pile with a difference in water depth across the structure, it may be possible that a similar effect may enhance the flow around piles. This could result in larger current velocities than those given by the shallow water relationship (i.e., maximum current velocity larger than 5.9 m/s for a water depth of 3.5 m), this would increase the upward bound of predicted scour than what is shown here.

Regardless, underestimating either of these parameters may lead to inaccuracies in the scour equations used here. A significantly higher flow velocity will ultimately result in deeper scour depths. An increase in wave period leads to an increase in the *KC* number, which may not strictly increase the scour depth as the wave scours out a larger area compared with a smaller *KC* number (Sumer and Fredsøe 2002). This may indicate that uncertainty in either of these parameters could be a source of underprediction.

Pore Pressure and Liquefaction

Considering the grain-size distribution, median grain size, C_u and C_c values, sediments from Cannon Beach, Yakutat, AK, and Mexico Beach, FL, were similar for the purpose of this study. Both sediments contained a negligible amount of fine grains (grains smaller than 0.075 mm) and may have had permeabilities of similar magnitude. The largest difference between these two sediments was the specific gravity with the Cannon Beach, AK, sediment being 1.1 times larger than the Mexico Beach, FL, sediment. This would imply that for similar sediment conditions, the Cannon Beach, AK, sediment would require a larger excess pore-pressure difference to induce liquefaction (Mory et al. 2007).

Figs. 11 and 12 show that the excess pore-pressure head differences that occurred at Cannon Beach, AK, were sufficiently large to overcome the liquefaction criteria determined by the laboratory experiments for the Mexico Beach, FL, sediments and the Mory et al. (2007) equation using the Mexico Beach, FL, and Cannon Beach, AK, sediments. The wave heights and water depths for the Cannon Beach, AK, data (0.58–0.83 m, 0.63–1.3 m, respectively) were smaller than the maximum values reported by in situ measurements at Mexico Beach, FL, from Hurricane Michael (2 m, 3.5 m, respectively) (Kennedy et al. 2020; USGS 2020). In addition to the less energetic conditions of the Cannon Beach, AK, sediment, the Mexico Beach, FL, sediment surrounding the piles tested in this study were significantly farther away from the shoreline (~100–350 m). The Mexico Beach, FL, sediments were, in all likelihood, drier and looser before their inundation than the Cannon Beach, AK, sediments. This implies a larger gas content and porosity for the Mexico Beach, FL, sediments than the Cannon Beach, AK, sediments prior to the Mexico Beach, FL, sediment inundation.

From these differences in sediment conditions, it could be said that the Mexico Beach, FL, sediment would have an increased risk of liquefaction compared with the Cannon Beach, AK, sediment (Yamamoto et al. 1978; Sakai et al. 1992; Mory et al. 2007). Since Cannon Beach, AK, had possible liquefaction events under less energetic conditions than the Mexico Beach, FL, sediment, it is a feasible hypothesis that the more at risk of liquefaction Mexico Beach, FL, sediment experienced liquefaction events under the more energetic Hurricane Michael conditions. Furthermore, liquefaction may occur more often in normally emerged locations far from the shoreline when rapidly inundated compared with normally submerged sediments due to the emerged location's looser (high porosity) and drier (high gas content) sediments (Yamamoto et al. 1978; Sakai et al. 1992; Mory et al. 2007).

Figs. 11 and 12 show that more liquefaction events occurred during the ebb- rather than the high tide. The larger amount of attenuation found in the ebb- compared with the high tide (Figs. 13 and 14) may imply that the risk of liquefaction at ebb tide is greater, resulting in more liquefaction events. A more attenuated signal implies a larger magnitude in the excess pore-pressure gradient, thus increasing the risk of momentary liquefaction (Yamamoto et al. 1978; Sakai et al. 1992; Mory et al. 2007). The increased attenuation in Fig. 13 and larger amount of liquefaction events for the ebb tide data (Figs. 11 and 12) may be a result of the changes in gas content from high- to ebb tide as previously discussed (Yamamoto et al. 1978; Mory et al. 2007). Furthermore, waves may have become steeper during the ebb tide. This would change the appearance of the wave crest and trough and thus have an impact on the development of excess pore-pressure gradients (Stark 2017).

Conclusion

The depth of scour holes at 30 piles caused by Hurricane Michael was measured in inundated areas at Mexico Beach, FL. The observed scour hole depths were compared against the results of five prediction equations. It should be highlighted that the scour holes were located inland [100–350 m from coastline; see in Fig. 2(d)] in areas inundated during Hurricane Michael, while the scour prediction equations were developed for riverine (Froehlich 1988; FHWA 2012) and offshore environments (Sumer et al. 1992; Sumer and Fredsøe 2002). Soil samples at Mexico Beach, FL, were collected and tested in the laboratory to characterize the sediment and to determine the excess pore-pressure head difference required to liquefy the soil. This was then compared with the theoretical liquefaction pressure given by Mory et al. (2007). The possibility of occurrence of these excess pore-pressure gradients was assessed using field data collected in Yakutat, AK, during moderate wave conditions (wave heights of 0.58–0.83 m in water depths of 0.63–1.3 m). Finally, the pore-pressure dissipation model as presented by Yamamoto et al. (1978) was compared with field data to observe the wave-induced excess pore-pressure attenuation behavior during different phases of the tide. The first goal of this study was to test common scour prediction equations for the special scenario of scour under hurricane inundation of onshore areas in the case of Mexico Beach, FL, during Hurricane Michael. The second goal was to investigate the feasibility of momentary liquefaction as a mechanism enhancing scour and thus as a possible explanation for some of the observed underprediction of scour. The following conclusions can be drawn.

The equations were generally able to provide predicted scour depths that are equal to or greater than the measured scour depth (Figs. 7–10). However, in 42 of the total 120 (35%) prediction iterations (Table 8), the predicted scour depths were smaller than the observed scour depths, representing an underprediction and undesired risk. Momentary liquefaction was found to be one possible contributor to and explanation for this discrepancy. Other explanations include, but are not limited to, unknown soil and

hydrodynamic conditions or that are outside the range of a specific equation, breaking waves, complex flow geometry, the refilling of scour holes after their development, and other physical processes that are not accounted for by the equations.

From a combination of laboratory liquefaction tests and field data, it appears possible that momentary liquefaction occurred and enhanced local scour in inundated areas during Hurricane Michael. Rapid inundation time may have left the soil with an above average gas content, which may have increased the likelihood of momentary liquefaction (Yamamoto et al. 1978; Sakai et al. 1992; Mory et al. 2007). The field data from Yakutat, AK, suggest that the difference in excess pore-pressure head between two sediment layers (with sediment properties characteristic of Yakutat, AK, as well as Mexico Beach, FL) caused by the troughs of ordinary- and infragravity waves was large enough to cause momentary liquefaction. Additionally, the data showed that there were more instances of momentary liquefaction during shallow water conditions (0.68 m water depth). This supports the premise that momentary liquefaction during inundation and storm conditions could have exacerbated the effects of scour and possibly contributed to the development and depth of onshore scour holes during Hurricane Michael in Mexico Beach, FL.

The scale of this study, the difficulty in predicting hurricane landfall, and the risks associated with deploying sensors in hurricane conditions prevented a wide range of scour prediction equations and their respective parameters being tested. The results of this study represent a first examination of the processes and other factors contributing to scour formation around onshore-located round and square piles due to hurricane-induced inundation. The possibility of momentary liquefaction as a likely source of the discrepancy between measured scour holes and predictions of scour from existing equations was considered. Future and larger scale studies should consider a wider range of equations (e.g., slender piles, pile groups, around structures) and the necessary measurements for the respective input parameters (e.g., wave period, boundary layer thickness, the refilling of scour holes). Additionally, to tackle the uncertainties of scour enhancement by return flow (e.g., Yeh and Mason 2014) or inundation velocities (e.g., Matsutomi et al. 2011), focus should be on the directionality of debris to determine whether they were deposited by return or inundating flows.

Data Availability Statement

Some or all data, models, or code that support the findings of this study are available from the corresponding author upon reasonable request. Additionally, field and laboratory data used for this study are in preparation to be made publicly available through the DesignSafe-CI data repository and are currently available upon request by the author.

Acknowledgments

The authors acknowledge funding from the National Sciences Foundation through grants CMMI- 1822307 and CMMI-1751463. The authors also acknowledge and thank Andrew Copp, Anderson Gradel, Kurtis Gurley, Matt Janssen, James Kaihatu, Douglas Krafft, Patrick Lynett, Margaret Ownesby, Jean-Paul Pinelli, David Prevatt, Spencer Rogers, David Roueche, and Zachariah Silver for their work in collecting the data. The authors would also like to thank three anonymous reviewers for detailed feedback that contributed to the improvement of this manuscript.

References

Albatal, A., N. Stark, and B. Castellanos. 2020. "Estimating in situ relative density and friction angle of nearshore sand from portable free-fall penetrometer tests." *Can. Geotech. J.* 57 (1): 17–31. https://doi.org/10.1139/cgj-2018-0267.

ASTM. 2014. *Standard test methods for specific gravity of soil solids by water pyncometer*. ASTM D854-14. West Conshohocken, PA: ASTM.

ASTM. 2017a. *Standard test methods for particle-size distribution (gradation) of soils using sieve analysis*. ASTM D6913-17. West Conshohocken, PA: ASTM.

ASTM. 2017b. *Standard practice for classification of soils for engineering purposes (unified soil classification system)*. ASTM D2487-17. West Conshohocken, PA: ASTM.

Beven II, J. L., R. Berg, and A. Hagen. 2019. "Hurricane Michael." National Hurricane Center Tropical Cyclone Report. Accessed March 28, 2020. https://www.nhc.noaa.gov/data/tcr/AL142018_Michael.pdf.

Bijker, E. W., and C. A. De Bruyn. 1988. "Erosion around a pile due to current and breaking waves." In *Coastal Engineering 1988*, 1368–1381. Reston, VA: ASCE. https://journals.tdl.org/icce/index.php/icce/issue/view/143.

Borga, M., B. F. Tanyu, C. M. Ferreira, J. L. Garzon, and M. Onufrychuk. 2017. "A geospatial framework to estimate depth of scour under buildings due to storm surge in coastal areas." *J. Nat. Hazards* 87 (3): 1285–1311. https://doi.org/10.1007/s11069-017-2817-3.

Bostick, K. W., S. A. Johnson, and M. B. Main. 2005. "Florida's geological history." Accessed August 29, 2019. http://edis.ifas.ufl.edu/uw208.

Carreiras, J., P. Larroudé, F. Seabra-Santos, and M. Mory. 2000. "Wave scour around piles." In *27th Int. Conf. on Coastal Engineering*, edited by B. L. Edge, 1860–1870. Reston, VA: ASCE.

Dean, R., and R. A. Dalrymple. 1991. *Water wave mechanics for engineers and scientists*. Hackensack, NJ: World Scientific.

Eid, W. K. 1987. "Scaling effect in cone penetration testing in sand." Ph.D. thesis, Dept. of Civil Engineering, Virginia Tech.

Falcone, F. T., and N. Stark. 2016. "Evaluation of the performance of sour prediction equations with regards to flow and sediment characteristics." In *Geo-Chicago 2016*, 671–680, Reston, VA: ASCE.

FDEP (Florida Dept. of Environmental Protection). 2019. "Geological maps and cross sections maps." *Florida Geological Survey*. Accessed August 29, 2019. https://ca.dep.state.fl.us/mapdirect/.

FHWA (Federal Highway Administration). 2005. *Field observations and evaluations of streambed scour at bridges*. FHWA-RD-03-052. Washington, DC: U.S. Dept. of Transportation.

FHWA (Federal Highway Administration). 2012. *Evaluating scour at bridges*. Washington, DC: FHWA.

Florence, M., and N. Stark. 2019. "Analysis of vertical pore pressure gradients in the lower intertidal zone." In *Proc., 9th Int. Coastal Sediments Conf.*, 2488–2499. Hackensack, NJ: World Scientific.

Froehlich, D. C. 1988. "Analysis of on-site measurements of scour at piers." In *Proc., 1988 National Conf. on Hydraulic Engineering*, edited by S. R. Abt and J. Gessler, 534–539. New York: ASCE.

Guest, T., and A. Hay. 2017. "Vertical structure of pore pressure under surface gravity waves on a steep, megatidal, mixed sand-gravel-cobble beach." *J. Geophys. Res. Oceans* 122 (1): 153–170. https://doi.org/10.1002/2016JC012257.

Holtz, R., W. Kouvacs, and T. Sheahan. 2017. *An introduction to geotechnical engineering*. Chennai, India: Pearson.

Lambe, W. T., and R. V. Whitman. 1969. *Soil mechanics*. New York: Wiley.

Lane, E. 1987. *Guide to rocks and minerals of Florida*. Tallahassee, FL: State of Florida, Dept. of Natural Resources.

Kennedy, A., et al. 2020. "Hurricane Michael in the Area of Mexico Beach, Florida." *J. Waterway, Port, Coastal, and Ocean Eng.* 146 (5): 05020004. https://doi.org/10.1061/(ASCE)WW.1943-5460.0000590.

Kobayashi, T., and K. Oda. 1994. "Experimental study on developing process of local scour around a vertical cylinder." In *Proc., 24th Int. Conf. on Coastal Engineering*, edited by B. L. Edge. Reston, VA: ASCE.

Matsutomi, H., K. Okamoto, and K. Harada. 2011. "Inundation flow velocity of tsunami on land and its practical use." In *Proc., of 32nd Conf. on Coastal Engineering*, edited by J. M. Smith and P. Lynett. Berkeley, CA: Council on Wave Research.

MBARA (Mexico Beach Artificial Reef Association). 2020. Accessed January 5, 2010. https://www.mbara.org/mexico-beach-artificial-reefs.cfm.

McGovern, D. J., D. Todd, T. Rossetto, R. J. S. Whitehouse, J. Monaghan, and E. Gomes. 2019. "Experimental observations of tsunami induced scour at onshore structures." *J. Coastal Eng.* 152: 103505. https://doi.org/10.1016/j.coastaleng.2019.103505.

Michallet, H., M. Mory, and I. Piedra-Cueva. 2009. "Wave-induced pore pressure measurements near a coastal structure." *J. Geophys. Res.* 114 (C6): 1–18. https://doi.org/10.1029/2008JC005071.

Mory, M., H. Michallet, D. Bonjean, I. Piedra-Cueva, J. Barnoud, P. Foray, S. Abadie, and P. Breul. 2007. "A field study of momentary liquefaction caused by waves around a coastal structure." *J. Waterway, Port, Coastal, Ocean Eng.* 133 (1): 28–38. https://doi.org/10.1061/(ASCE)0733-950X.

Munk, W. 1950. "Origin and generation of waves." In *Proc., 1st Int. Conf. on Coastal Engineering*, edited by J. W. Johnson. Berkeley, CA: Council on Wave Research.

Nielsen, A. W., B. M. Sumer, S. S. Ebbe, and J. Fredsøe. 2012. "Experimental study on the scour around a monopile in breaking waves." *J. Waterway, Port, Coastal Ocean Eng.* 138 (6): 501–506. https://doi.org/10.1061/(ASCE)WW.1943-5460.0000148.

NOAA (National Oceanic and Atmospheric Administration). 2019. "Assessing the U.S. Climate in 2018." Accessed July 1, 2019. https://www.ncei.noaa.gov/news/national-climate-201812.

NOAA (National Oceanic and Atmospheric Administration). 2020. "Data Access Viewer." Accessed January 5, 2020. https://coast.noaa.gov/dataviewer/?redirect=301ocm&keyword=lidar#/lidar/search/-9510237.731470415,3492832.0475067846,-9504160.987721743,3497892.179129164.

Paprocki, J., N. Stark, H. Graber, H. Wadman, and J. McNinch. 2021. "Assessment of moisture content in sandy beach environments from multispectral satellite imagery." *Can. Geotech. J.* 1–56. https://doi.org/10.1139/cgj-2020-0624.

Raubenheimer, B., S. Elgar, and R. Guza. 1998. "Estimating wave heights from pressure measured in sand bed." *J. Waterway, Port, Coastal, Ocean Eng.* 124 (3): 151–154. https://doi.org/10.1061/(ASCE)0733-950X(1998)124:3(151).

Sakai, T., K. Hatanaka, and H. Mase. 1992. "Wave-induced effective stress in seabed and Its momentary liquefaction." *J. Waterway, Port, Coastal, Ocean Eng.* 118 (2): 202–206. https://doi.org/10.1061/(ASCE)0733-950X(1992)118:2(202).

Schmidt, W., and M. Clark. 1980. *Geology of Bay County, Florida*. Bulletin No. 57. Tallahassee, FL: State of Florida, Dept. of Natural Resources.

Shields, A. 1936. *Application of similarity mechanics and turbulence research on shear flow*. [In German.] Mitteilungen der Preußischen Versuchsanstalt für Wasserbau. Berlin: Prussian Research Institute for Hydraulic Engineering.

Stark, N. 2017. "Pore pressure response to irregular waves at a sandy beach." In *Geotechnical Frontiers 2017: Geotechnical Materials, Modeling, and Testing*, Geotechnical Special Publication 280, edited by T. L. Brandon and R. J. Valentine, 409–417. Reston, VA: ASCE.

Stark, N., and B. Quinn. 2015. "Pore pressure monitoring of surficial coastal sediments on wave-resolving scale with outlook on liquefaction risk prediction at offshore wind and marine hydrokinetic energy converters." In *Proc., 2015 Int. OCEANS Conf.*, 1–7. New York: IEEE.

Sumer, B. M., and J. Fredsøe. 2001. "Scour around a pile in combined waves and current." *J. Hydraul. Eng.* 127 (5): 403–411.

Sumer, B. M., and J. Fredsøe. 2002. *The mechanics of scour in the marine environment*. Hackensack, NJ: World Scientific.

Sumer, B. M., J. Fredsøe, and N. Christiansen 1992. "Scour around a vertical pile in waves." *J. Waterway, Port, Coastal, Ocean Eng.* 117 (1): 15–31. https://doi.org/10.1061/(ASCE)0733-950X(1992)118:1(15).

Sumer, B. M., J. Fredsøe, and N. Christiansen. 1993. "Influence of cross section on wave scour around piles." *J. Waterway, Port, Coastal, Ocean Eng.* 119 (5): 477–495. https://doi.org/10.1061/(ASCE)0733-950X(1993)119:5(477).

Terzaghi, K., R. Peck, and G. Mesri. 1996. *Soil mechanics in engineering practice*. New York: Wiley.

USGS. 2020. "Flood event viewer." Accessed December 29, 2019. https://stn.wim.usgs.gov/fev/#MichaelOct2018.

Vanoni, V. 2014. *Sedimentation engineering*. Reston, VA: ASCE.

Yamamoto, T., H. Koning, H. Sellmeijer, and E. Hijum. 1978. "On the response of a poro-elastic bed to water waves." *J. Fluid Mech.* 87 (1): 193–206. https://doi.org/10.1017/S0022112078003006.

Yang, Y., and R. G. D. Davidson-Arnott. 2005. "Rapid measurement of surface moisture content on a beach." *J. Coastal Res.* 21 (3): 447–452. https://doi.org/10.2112/03-0111.1.

Yeh, H., and H. B. Mason. 2014. "Sediment response to tsunami loading: Mechanisms and estimates." *Géotechnique* 64 (2): 131–143.

Young, I. R. 2003. "A review of the sea state generated by hurricanes." *Mar. Struct.* 16: 201–218. https://doi.org/10.1016/S0951-8339(02)00054-0.